Quantum Paraelectricity in Double-Perovskites

Marlene Abshagen

Bachelor Thesis

Mathematisch-Naturwissenschaftliche Fakultät
Christian-Albrechts-Universität zu Kiel
2024

First Examiner: Prof. Dr. Fabio Caruso
Second Examiner: Prof. Dr. Michael Bonitz

Zusammenfassung

In einer klassischen Betrachtung eines Festkörpers existieren zwei Phasen der Polarisierung: die ferroelektrische Phase und die paraelektrische Phase. Nach der Landau Theorie lassen sich die Phasen durch unterschiedliche Potentiale beschreiben: die paraelektrische Phase kann durch eine Parabel dargestellt werden, während die ferroelektrische Phase durch ein „double-well“ Potential abgebildet werden kann.
Werden die Phasen der Polarisierung aus quantenmechanischer Sicht betrachtet, existiert aber noch eine dritte, weniger bekannte Phase: die quantenparaelektrische. Bei dieser wird der Übergang vom para- zum ferroelektrischen Zustand aufgrund von Quantenfluktuationen zwischen den Polarisierungszuständen unterdrückt. Es tritt ein „double-well“ Potential auf und es ergibt sich eine Delokalisierung der Aufenthaltswahrscheinlichkeit des Grundzustands aufgrund von Tunnelwahrscheinlichkeiten. Im Vergleich dazu ergibt sich im „double-well“ Potential der ferroelektrischen Phase eine Lokalisierung der Aufenthaltswahrscheinlichkeit des Grundzustands in einem der beiden Minima des Potentials.
Eine der bekanntesten quantenparaelektrischen Kristallstrukturen ist der Perowskitkristall Strontiumtitanat ($SrTiO_3$). Bei Raumtemperatur befindet sich der Kristall in einer kubischen Struktur. Dabei nehmen die Strontiumionen die Eckplätze ein, während sich das Titanion in der Mitte der Einheitszelle befindet. Wie bei allen Perowskiten bilden die Sauerstoffionen eine oktaedrische Form um das zentrale Ion.
Ausgehend von dieser Struktur wird in dieser Arbeit mit einer Methode, entwickelt von T. Esswein und N. Spaldin [1], gearbeitet, welche es ermöglicht, den quantenparaelektrischen Charakter unter anderem von $SrTiO_3$ zu berechnen. Die Methode basiert auf Dichtefunktionaltheorie und der Verwendung der Einteilchen Schrödinger-Gleichung.
Der Hauptfokus dieser Arbeit liegt auf Doppelperowskiten, welche sich aus zwei einfachen Perowskitstrukturen zusammensetzen. Viele Eigenschaften von einfachen Perowskiten lassen sich auf Doppelperowskite übertragen, wie ihre Anwendung im Photovoltaikbereich. In dieser Arbeit wird der Frage nachgegangen, ob sich das Phänomen der Quantenparaelektrizität auch in Doppelperowskiten wiederfindet.
Dafür wurde die Methode, mit welcher der quantenparaelektrischen Charakter von Strontiumtitanat untersucht werden konnte, auf 77 Doppelperowskite mit derselben elektronischen Konfiguration wie $SrTiO_3$ angewandt. Das Ergebnis führte auf zwei mögliche Kandidaten für quantenparaelektrische Doppelperowskite. Zudem wurden Hinweise auf einen geometrischen Ursprung von Quantenparaelektrizität gefunden.

Abstract

In a classical view of a solid, there exist two phases of polarization: the ferroelectric phase and the paraelectric phase. These phases can be described by different potentials, using Landau theory. The paraelectric phase can be described using a parabolic potential, whereas the ferroelectric phase can be depicted as a double-well potential. If these phases of polarization are viewed from a quantum mechanical point of view, there exists a third, less known phase: the quantum paraelectric one. In this phase the material is on the verge of transitioning to a ferroelectric state, however this transition is suppressed by quantum fluctuations between the polarized states. If this phase is described using a double-well potential, a delocalization of the probability density of the ground state across the whole potential would arise. In contrast, the probability density of a ferroelectric phase would result in a clear localization in one of the minima.
One of the best known quantum paraelectric materials is strontium titanate. At room temperature this perovskite has a cubic structure, where the strontium ions take the corner spaces, while the oxygen ions form an octahedral shape around the central titanium ion. Based on this structure, this thesis applies a method suggested by T. Esswein and N. Spaldin [1], which makes it possible to calculate the quantum paraelectric character of e.g. strontium titanate. This method is based on density functional theory and the one-particle Schrödinger equation.
The main focus of the thesis is on double perovskites, which consist of two simple perovskite structures combined. Many applications can be transferred from simple to double perovskites, like their use in photovoltaic technology. This thesis investigates whether the phenomenon of quantum paraelectricity can be found in double perovskites.
For this purpose 77 double perovskites of the same electronic configuration as strontium titanate were examined using the same method as for strontium titanate. The results identified two potential candidates for quantum paraelectric materials. Additionally, indications of a geometric origin of quantum paraelectricity were found.

Contents

Chapter 1

Introduction

In recent years perovskites have become more and more important: they are one of the most versatile families of crystals with a very large collection of properties. Among other things, they show metallic, insulating and semiconducting behaviour, but also superconducting, ferromagnetic or ferroelectric phases can be found [2]. Perovskites are central to many areas of current research. One example is their application in solar cells: they already achieve efficiencies of over 25%, despite having only been researched for about a decade. Laboratory-made small solar cells are able to match the efficiency of monocrystalline silicon solar cells, which currently dominate the global photovoltaic technology market [3].
The structure of all perovskites is the same: they consist of molecules of the structure ABX_3, where A and B are cations and X is an anion. The B-cation of the structure is located in the center of the unit cell, while the X-anions are arranged in an octahedral shape around the central cation. The A-cation is located on the edges of the unit cell. The general perovskite structure is illustrated by the example of strontium titanate in fig. 1.1.
While this composition is found in all perovskites, the perovskite structures can differ in the degree of tilting of the octahedron and therefore a distortion of the structure, which can result in different stability behaviors of the compounds. These stability behaviors can be described by geometric factors. For a simple perovskite of the ABX_3

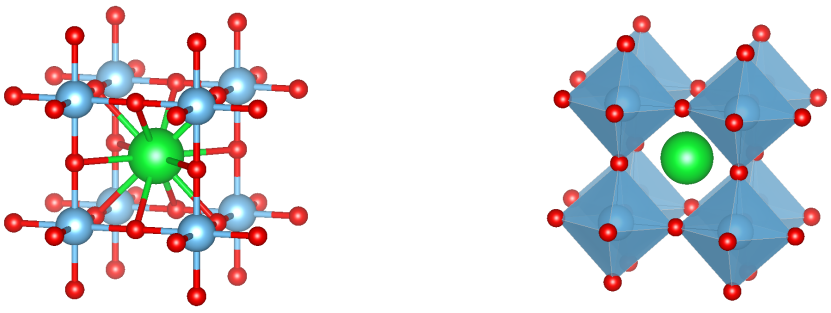

Figure 1.1: **Left**: Strontium titanate ($SrTiO_3$) with oxygen anions (red) in an octahedral form around the titanium cation (green). The strontium cations (blue) are located at the edges of the cubic cell. Here the bonds of the structure are shown.
Right: Oxygen octahedra (blue) with titanium ion (green) in the middle in strontium titanate. [4]

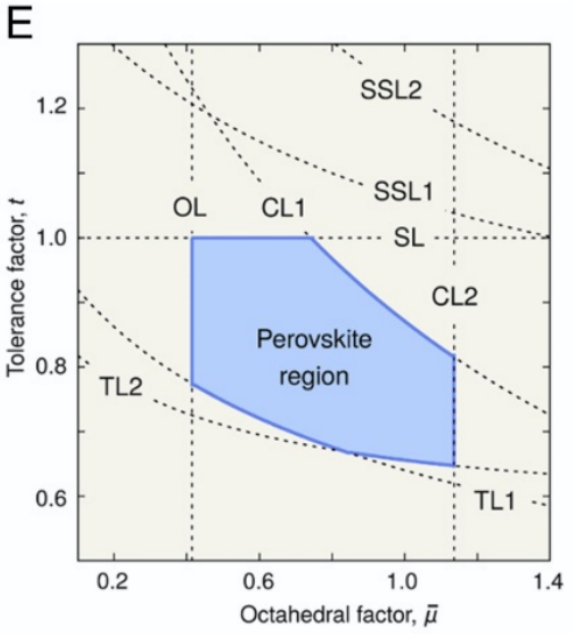

Figure 1.2: Stability region of perovskites (blue), which is dependent on the tolerance factor as well as the octahedral factor. It is constrained by several limitations, like the chemical limits (CL1, CL2), octahedral limits (OL), stretch limits (SL), secondary stretch limits (SSL1, SSL2), and tilt limits (TL1, TL2). With this region it is possible to predict the stability of a random perovskite. [2] (fig. 1.E)

structure they are given by the tolerance factor t_s and the octahedral factor μ, which are dependent on the ionic radii of the ions [2]. Together, these two factors define a region in parameter space, in which perovskite structures are stable, as illustrated in fig. 1.2. The dashed lines in fig. 1.2 indicate various limitations, such as chemical limits (CL1, CL2), octahedral limits (OL), stretch limits (SL), secondary stretch limits (SSL1, SSL2), and tilt limits (TL1, TL2). The octahedral factor provides detail on the ration of the size of the octahedral anions surrounding the central cation. The tolerance factor gives information about in which structural phase a perovskite is present. For an idealized cubic perovskite the tolerance factor should equal one. However, distortions in the structure lead to a different tolerance factor [5]. If the tolerance factor is smaller than one, the three different-sized ions are "packed" in such a way that they do not occupy the entire space, leaving gaps. This occurs because the A-site ions are too small to occupy the full space. The octahedron can rotate slightly, leading to deviations from the cubic structure. These factors are useful tools when researching perovskites.

Besides simple perovskite structures, there also exist double perovskites, composed of two simple perovskites. They have a crystal structure of the form AA'BB'X_6, where A and A' are alkaline earth and/or rare earth metals and B and B' are transition metals [6]. An example for a double perovskite is Sr_2LaNbO_6, depicted in fig. 1.3, with the central niobium ion (yellow), lanthanum ions (purple) at the corners of the structure, strontium ions (green), and the oxygen ions (red) arranged octahedrally around the corner atoms and the central atom. As with simple perovskite structures, a tolerance factor and an octahedral factor can be determined for double perovskites.

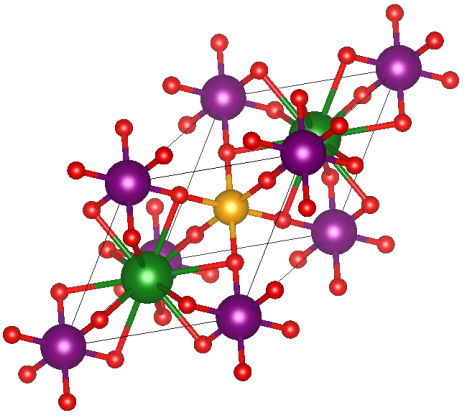

Figure 1.3: Double Perovskite Structure of Sr_2LaNbO_6 with lanthanum ions (purple), strontium ions (green), niobium ion (yellow), and oxygen ions (red). [4]

However, since there now exist two different cations, B and B', there are two octahedral parameters to be taken into account: the average octahedral factor $\bar{\mu}$ and the octahedral mismatch $\Delta\mu$, which, similar to simple perovskite structures, characterize the stability together with the tolerance factor t.
The reason why double perovskites are highly interesting structures can be illustrated in analogy to simple perovskite structures on the example of solar cell research: while simple perovskite solar cells are attractive due to their low-cost production and high efficiency, they face challenges such as material toxicity, device hysteresis, and stability issues [7]. Double perovskites present a promising solution: they can be fabricated from lead-free materials like halides and oxides, thereby enhancing their environmental friendliness. Moreover, combining two perovskite structures into a double perovskite often results in improved stability, optoelectronic properties, and thermal conductivity [8].
Perovskites are therefore an extremely interesting group of compounds. Besides their applications in solar cells, they also offer other remarkable properties. A particularly intriguing example is strontium titanate. This material is classified as quantum paraelectric, meaning that it is near the transition to a ferroelectric state but does not become ferroelectric at low temperatures due to quantum mechanical fluctuations between two opposite polarization states. This unique property makes strontium titanate an important subject of study in solid state physics and materials science.

Many characteristics of simple perovskite structures, like the application in the photovoltaic sector, can thus be transferred to and partially optimized in double perovskites. But what about the phenomenon of quantum paraelectricity?
This thesis investigates whether quantum paraelectricity can occur in double perovskites. To address this question, a method proposed by T. Esswein and N. Spaldin [1] was used to identify the quantum paraelectric character of strontium titanate. First the numerical code is verified by comparison with the values for strontium titanate from [1]. This method was then applied to a bulk of 77 double perovskites of the same electronic configuration as strontium titanate and the results were evalu-

ated. Additionally, the question, whether there exists a geometric origin of quantum paraelectricity in double perovskites, was pursued.

Chapter 2

Density Functional Theory (DFT)

2.1 Basics of the Density Functional Theory

Density Functional Theory is a way of solving the non-relativistic, time-independent Schrödinger equation. It is the most commonly used method to investigate ground state properties of any material. DFT calculations form the basis of this thesis. A brief overview of the most important principles of DFT is given in this chapter. The derivations in this chapter follow "Materials Modeling using Density Functional Theory" by Feliciano Giustino [9].

2.1.1 Many Body Hamiltonian

Every type of matter, whether solid or molecule, can be broken down to the fact that it can be composed of a finite number of electrons and nuclei. This system can be described by a many-body wave function Ψ_s, which depends on the positions $\vec{R}_I$ of the nuclei and their spins Σ_I, as well as the positions $\vec{r}_i$ and spins σ_i of the electrons. The s in the index of the wave function describes the corresponding energy eigenstate. $I = 1, ..., N_n$ and $i = 1, ..., N$ applies, where N_n is the total number of nuclei and N is the total number of electrons. In the following, however, the electronic and nucleon spin is neglected. The general wave function would still depend on the time, but since the interest is usually on the stationary state when calculating the ground state properties of a system, the wave function can be reduced to $\Psi_s(r, R)$.
The wave function obeys the time-independent Schrödinger equation

$$\hat{\mathcal{H}}\Psi_s = E_s\Psi_s\,,$$

with the energy levels E_s of the system. The Hamilton operator of the system is composed of the kinetic energy of the electron $\hat{T}_e$, the kinetic energy of the nucleons $\hat{T}_n$, as well as the potential energy resulting from the Coulomb interaction between the electrons $\hat{V}_{ee}$, the Coulomb interaction between the nucleons themselves $\hat{V}_{nn}$ and the Coulomb interaction between the electrons and the nucleons $\hat{V}_{en}$. This results in [9]

$$\hat{\mathcal{H}} = \hat{T}_n + \hat{T}_e + \hat{V}_{nn} + \hat{V}_{ee} + \hat{V}_{en}\,. \tag{2.1}$$

Hartree Atomic Units

To simplify the expressions for the operators, the Hartree Atomic Units are used for the following equations. These are defined via

$$\hbar = m_e = e^2 = \frac{1}{4\pi\epsilon_0} = 1\,,$$

where $\hbar$ is the reduced Planck constant, m_e the electron mass, e the electron charge and ϵ_0 the vacuum permittivity. This has the advantage that the Coulomb interaction between a particle at location $\vec{r}$ and another particle at location $\vec{r}\,'$ is reduced in SI units as follows

$$\frac{e^2}{4\pi\epsilon_0|\vec{r}-\vec{r}\,'|} \mapsto \frac{1}{|\vec{r}-\vec{r}\,'|}$$

The individual operators from eq. (2.1) for a system of N electrons and N_n nucleons can now be written as

$$\hat{\mathcal{H}} = \underbrace{-\sum_i^N \frac{\nabla_i^2}{2}}_{\hat{T}_e} \underbrace{-\sum_I^{N_n} \frac{\nabla_I^2}{2M_I}}_{\hat{T}_n} + \underbrace{\frac{1}{2}\sum_{i\neq j}^{N} \frac{1}{|\hat{\vec{r}}_i - \hat{\vec{r}}_j|}}_{\hat{V}_{ee}} + \underbrace{\frac{1}{2}\sum_{I\neq J}^{N_n} \frac{Z_I Z_J}{|\hat{\vec{R}}_I - \hat{\vec{R}}_J|}}_{\hat{V}_{nn}} \underbrace{-\sum_i^N \sum_I^{N_n} \frac{Z_I}{|\hat{\vec{r}}_i - \hat{\vec{R}}_I|}}_{\hat{V}_{en}}\,,$$

with i, j as an index referring to the electrons and I, J to the nuclei. Thus M_I is the mass of the I-th ion, ∇_I and ∇_i are respectively the gradient for the nuclei at $\vec{R}_I$ and the electron at $\vec{r}_i$. Z_I is the atomic number of the I-th ion.
With this Hamiltonian, the stationary Schrödinger equation 2.1.1 can be solved exactly for simple systems, such as a free electron in a vacuum or the hydrogen atom. If the system contains more components, such as molecules or crystalline solids, the solution can only be approximated by numerical simulations.

2.1.2 Hohenberg Kohn Theorems

One of the most important foundations for density functional theory was presented by Hohenberg and Kohn in 1964 in the form of two theorems. The first theorem states that [10]

> **The external potential $\hat{V}_{en}$ is a unique functional of the ground state electron density $n(\vec{r})$.**

This theorem implies that for any given external potential $\hat{V}_{en}$ there can exist exactly one electron density $n(\vec{r})$ and, on the other hand, for a given density $n(\vec{r})$ there can exist only one external potential $\hat{V}_{en}$. Accordingly, two systems with the same number of electrons but two different external potentials also have different electron densities.
For $\hat{V}_{en}$ the "clamped nuclei approximation" was applied: in this approximation the nuclear motion is neglected, since it can be assumed that the nucleus is mostly confined to a limited space and oscillates around an equilibrium position. Additionally, the masses of the nuclei are much bigger in comparison to those of the electrons, leading

to much slower movement. This means that the nuclei can be regarded approximately as rigid, making the positions of the nucleons a fixed parameter. Because of this, $\hat{V}_{en}$ takes the form of an external potential, depending only on one electronic position operator.
The significance of this discovery lies in the fact that this theorem brings the density into a direct correlation with the many-electron ground state energy, which in turn allows any quantity that depends on the functional of the ground state wave function to be expressed in terms of a functional of the density. For example, the ground state energy E can be written as follows [11]

$$E[n] = F[n] + \int d\vec{r}\, V_{en}(\vec{r}) n(\vec{r})\,, \tag{2.3}$$

with the density functional $F[n] = \langle \Psi_s | \hat{T} + \hat{V}_{ee} | \Psi_s \rangle$, where $\hat{T}$ is the kinetic energy operator for the electrons and $\hat{V}_{ee}$ is the Coulomb energy operator for two electrons. Both operators, $\hat{T}$ and $\hat{V}_{ee}$, are independent of the nuclear coordinates and only depend on the number of electrons N in the system. Therefore, $F[n]$ is an universal functional of the density. The second theorem states that [10]

The total energy E[n] is minimized at the N-electron ground state density $n(\vec{r})$.

This theorem connects the ground state energy to the electronic ground state density $n(\vec{r})$ in such a way, that the functional E[n] alone is sufficient to determine the ground state density [10].

2.1.3 Kohn Sham Equations

While the Hohenberg-Kohn theorems state that the ground-state energy uniquely dependent on the functional for the electron density and that the total energy is minimized at the ground-state density, they do not provide guidance on how to build such a functional. Equation (2.3) shows that the kinetic as well as the Coulomb energy operator for two electrons only depend implicitly on the density n. This lead Kohn and Sham 1965 to the hypothesis to split the terms, which are only implicitly density-dependent, into the kinetic energy and Coulomb energy of independent electrons, and adding an extra term, the exchange and correlation energy, which accounts for the difference [12]. This resulted in

$$E = F[n] = \underbrace{\int d\vec{r} n(\vec{r}) V_n(\vec{r})}_{\text{External Potential}} - \underbrace{\sum_i \int d\vec{r} \Phi_i^*(\vec{r}) \frac{\vec{\nabla}^2}{2} \Phi_i(\vec{r})}_{\text{Kinetic Energy}} + \underbrace{\frac{1}{2} \int\int d\vec{r} d\vec{r}\,' \frac{n(\vec{r}) n(\vec{r}\,')}{|\vec{r} - \vec{r}\,'|}}_{\text{Hartree Energy}} + \underbrace{E_{xc}[n]}_{\text{Exchange-Correlation energy}}\,,$$

with the orthonormal wavefunctions Φ_i. This equation divides the terms into the known contributions (total energy in the independent electrons approximation) and

the unknown component (exchange-correlation energy). The Hartree energy is a classical mean field contribution.
Thus, if the exchange-correlation energy and the electron density is known, it is possible to calculate the ground state energy.
The "Hohenberg-Kohn" variation principle (Hohenberg and Kohn, 1964) states that the ground state density n_0 is exactly the function that minimizes the total energy. This can be expressed as

$$\left.\frac{\delta F[n]}{\delta n}\right|_{n_0} = 0\,.$$

This results in [12]

$$\left[-\frac{1}{2}\vec{\nabla}^2 + V_{tot}(\vec{r})\right]\Phi_i(\vec{r}) = \epsilon_i\Phi_i(\vec{r}) \tag{2.4}$$

with orthonormal wave functions Φ_i and

$$V_{tot}(\vec{r}) = V_n(\vec{r}) + V_H(\vec{r}) + V_{xc}(\vec{r})\,.$$

Here, $V_{tot}(\vec{r})$ is the total potential, which is composed of the nuclear component $V_n(\vec{r})$ and the Hartree potential $V_H(\vec{r})$. The exchange-correlation potential is defined via

$$V_{xc}(\vec{r}) = \frac{\delta E_{xc}[n]}{\delta n}(\vec{r})\,. \tag{2.5}$$

The nuclear potential is given by

$$V_n(\vec{r}) = -\sum_I \frac{Z_I}{|\vec{r} - \vec{R}_I|}$$

and the Hartree potential can be derived by solving the Poisson equation

$$\vec{\nabla}^2 V_H(\vec{r}) = -4\pi n(\vec{r})\,. \tag{2.6}$$

The Hartree energy than can be calculated by

$$E_H = \frac{1}{2}\int d\vec{r}\; n(\vec{r})V_H(\vec{r})\,.$$

The density $n(\vec{r})$ can be determined through

$$n(\vec{r}) = \sum_i |\Phi_i(\vec{r})|^2\,. \tag{2.7}$$

This set of equations, from eq. 2.4 to 2.7, is known as the Kohn-Sham equations. However, they can't be solved exactly, which is the reason why an approximation has to be found. If a good approximation for the exchange correlation energy can be found, the Kohn-Sham theory is extremely useful for ground state DFT.

Local Density Approximation

One way to approximate the exchange correlation functional is the Local Density Approximation (LDA). This approximation uses the homogeneous electron gas (HEG) as a model to describe the exchange and correlation energy in regions where the density varies slowly. In the HEG model, it is assumed that the electrons do not interact with each other. The potential created by the nuclei is assumed to be constant and the N electrons are confined to a fixed volume V. The approximation now works in such a way that the electron density $n(\vec{r})$ in a solid is divided into regions, whereby the width is reduced to infinitesimally small volume elements. As a result, each infinitesimally small volume element $d\vec{r}$ can be approximated with the local homogeneous electron density $n(\vec{r})$, for which the exchange energy E_X and the correlation energy E_C can be calculated through [9]

$$E_X = -\frac{3}{4}\left(\frac{3}{\pi}\right)^{\frac{1}{3}} n^{\frac{4}{3}} V$$

$$E_C = nV \cdot \begin{cases} 0.0311\ln(r_s) - 0.0480 + 0.002 r_s \ln(r_s) - 0.0116 r_s, & \text{if } r_s < 1, \\ \frac{-0.1423}{\sqrt{1+1.0529 r_s + 0.3334 r_s}}, & \text{if } r_s \geq 1. \end{cases}$$

Here, n is the electron density with $n = \frac{N}{V}$, where N is the number of particles and V is the volume.
As there is no analytical expression for the correlation energy, it was solved using stochastic methods. In this case, r_s is the Wigner-Seitz radius, which is defined via

$$\frac{V}{N} = \frac{4\pi}{3} r_s^3 = \frac{1}{n}\,.$$

Once the exchange and correlation energies have been calculated for all subregions they are summed up, which results in $E_{xc}^{HEG}[n(\vec{r})]$. The exchange correlation energy of the entire system can then be calculated via

$$E_{xc} = \int_V dE_{xs} = \int_V \frac{E_{xc}^{HEG}[n(\vec{r})]}{V} d\vec{r}\,. \tag{2.8}$$

With eq. (2.8) all summands of the Kohn-Sham equations are now determined. The LDA is one of the most frequently used approximations for modern first-principles calculations.

2.2 Implementation of DFT

In a real crystal structure, there exist on average $\approx 10^{20}$ atoms in a cubic millimeter, which makes numerical calculations extremely difficult. At such a large scale, however, there are periodicities in the crystal that can be cleverly exploited. In order to be able to carry out calculations for real systems, various approximations and symmetries are now used to solve the problems self-consistently. This chapter introduces the Bloch theorem, pseudopotentials and self-consistent field calculations.

2.2.1 Bloch Theorem

If the nuclei are in a periodic arrangement, the potential V acting on the electrons must also be periodic. In this case, $V(\vec{r}+\vec{L}) = V(\vec{r})$ applies, where $\vec{L}$ is a lattice vector, describing the translational periodicity. Therefore the density $n(\vec{r})$ must also be periodic with $n(\vec{r}+\vec{L}) = n(\vec{r})$. Since the wave function is related to the density via $n(\vec{r}) = |\Phi(\vec{r})|^2$, the magnitude of the wave function is periodic as well, but its phase does not have to be periodic. If such a periodic potential is present, Bloch's theorem states that the wave functions can be expressed as [10]

$$\Psi_k(\vec{r}) = e^{i\vec{k}\cdot\vec{r}} u_k(\vec{r})$$

where $u_k(\vec{r}+\vec{L}) = u_k(\vec{r})$ is a periodic function that has the same periodicity as the crystal structure. $e^{i\vec{k}\cdot\vec{r}}$ is an arbitrary phase factor, describing a plane wave with wave vector $\vec{k}$.
In order to represent the wave functions, a suitable basis set must be selected. Since this is a periodic problem, u_k is described by a three-dimensional Fourier series with

$$u_k(\vec{r}) = \sum_G c_{Gk} e^{i\vec{G}\cdot\vec{r}},$$

where c_{Gk} are complex Fourier coefficients [13]. $\vec{G}$ is a reciprocal lattice vector for which, by definition, $e^{i\vec{G}\cdot\vec{L}} = 1$ applies. Each of the basis functions $e^{i\vec{G}\cdot\vec{r}}$ represents a plane wave that propagates perpendicular to the reciprocal lattice vector. There are an infinite number of $\vec{G}$ that fulfill this condition, but the coefficients c_{Gk} decrease more and more as $|G|^2$ becomes larger. It therefore makes sense to define a cutoff energy, which ensures that only plane waves with energies smaller than the cutoff are included. This cutoff energy constrains the number of needed values for $\vec{G}$ through the condition $\frac{\hbar^2}{2m}|\vec{G}|^2 < E_{\text{cutoff}}$. The respective cutoff energy for a structure can be determined using convergence tests, for which the cutoff energy is changed until the total energy of the system converges.

2.2.2 Pseudopotentials

Pseudopotentials are effective potentials that reproduce all electron wave functions beyond a cutoff radius [14]. This has the big advantage that it reduces the number of plane-wave basis sets, thus speeding up the calculation [15]. It also reduces the number of electrons and can include relativistic effects [13]. In the construction, the wave function to be simplified is divided into a core region, meaning the region closer to the nucleus, and a valence region. To obtain the pseudopotential, a wave function is now developed in such a way, that it is smooth close to the core and the valence zone. This can be seen in fig. 2.1 (left). With this wave function and the Schrödinger equation, a potential can be found that reproduces the wave function. Taking the Coulomb potential as an example, which is proportional to Z/r with the distance r and the atomic number Z, this potential diverges for $r \to 0$ against ∞. The pseudopotential is now constructed in such a manner, that this divergence does not occur, so it differs from the Coulomb potential in this region, but it matches the potential after the cutoff radius in the region where $r \to \infty$ applies. This is shown in

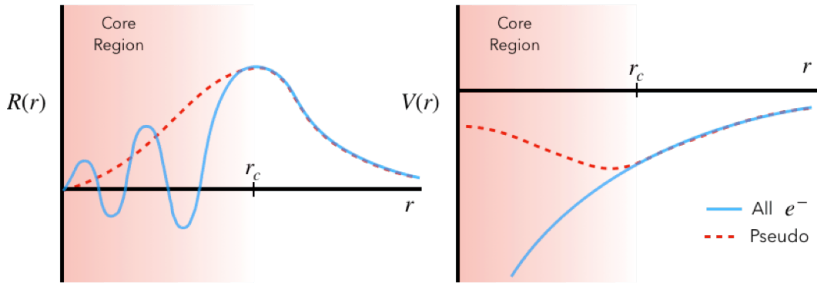

Figure 2.1: **Left**: Radial wave function $R(r)$ of the pseudo- (red dashed line) and the all electron wave function (blue line) dependent on the distance r. In the core region the wave function is a smooth curve, varying from the all electron wave function. After the cutoff radius r_c, both wave functions coincide. This region is called the valence region.
Right: The pseudopotential (red dashed) and the all-electron potential (blue). After the cutoff energy the pseudopotential and the all-electron potential coincide once again. Image from https://sites.psu.edu/dftap/2019/03/31/transferability-of-cu-pseudopotentials-in-cucuo-systems/

fig. 2.1 (right).
There are different classifications for pseudopotentials: if they are labeled "soft", then only a small number of Fourier components are required for an accurate representation of the potential, otherwise they are considered "hard". There also exist "ultrasoft" pseudopotentials, which were introduced by Vanderbuilt in 1990 [13]. With these, the pseudo wave function is made as "soft" as possible near the core, which allows the cutoff energy to be drastically reduced. It also provides good scattering properties over a pre-specified energy range, resulting in better accuracy.

2.2.3 Self-Consistent Field Calculations

To calculate the total energy from the Kohn-Sham equations, the principle of self-consistent field calculation is used. The term 'self-consistent' in this case stems from the fact that the solution of eq. (2.4), which results in the eigenfunctions $\Phi_i(\vec{r})$ and the eigenenergies ϵ_i, depends on the total potential $V_{tot} = V_n + V_H + V_{xc}$. Two components of this, V_H and V_{xc} (see eq. (2.6) and (2.5)), depend on the density, which in turn is dependent on the eigenfunctions $\Phi_i(\vec{r})$ (see eq. (2.7)). This whole circle of dependencies gives the calculation its self consistent character.
In order to obtain the energy from this chain of equations, nuclear coordinates are first determined, with which the nuclear potential V_n can be calculated. Now a possible electron density $n(\vec{r})$ is guessed, by for example adding up the densities of the individual atoms, taking into account their atomic position in the material. With this density, it is now possible to find approximations for the exchange-correlation potential V_{xc} as well as the Hartree potential V_H. The sum of the three potentials defines the total potential, with which a numerical solution of the Kohn-Sham equations can now be found. The result are the wave functions Φ_i, which can now be used to calculate the density. If the newly calculated density matches the initial guess within a tolerance interval, self-consistency has been achieved and it is now possible

to calculate the total energy of the system. If the newly calculated density still does not match the initial guess, a new guess is made for a new density, with which the process is repeated. This is done until self-consistency is achieved [9]. The whole procedure is shown in fig. 2.2.

2.3 Quantum ESPRESSO

Quantum ESPRESSO, founded by the Quantum ESPRESSO Foundation, is a free software package for electronic structure calculations of molecular systems at the nano scale [16]. With the help of this program, which is based on density functional theory, plane waves and pseudopotentials, the total energy of a system, phonon dispersions, density of states or band structures can be calculated for a material. The basic package includes "PWscf" (Plane Wave Self-Consistent Field), which solves the Kohn-Sham equations self-consistently. It also contains "PHonon," where Density Functional Perturbation Theory is applied, allowing for the calculation of second and third derivatives of energy based on atomic displacement. Additionally, "PostProc" enables data analysis and plotting. ESPRESSO is an acronym for "opEn-Source Package for Research in Electronic Structure, Simulation, and Optimization".
The suite works based on input files, where the kind of the calculation has to be defined as well as various parameters, describing the crystal structure. Examples of these parameters include the cell parameter, the atomic positions, the k-point grid on which the calculation runs, and many others. The pseudopotentials to be used for the calculation are also specified here. Quantum ESPRESSO generates so-called 'output' files containing the results of the calculation after the calculation has been successfully completed. In this thesis the Quantum ESPRESSO "Version 7.3", which was released on the 09.01.2024, was used.

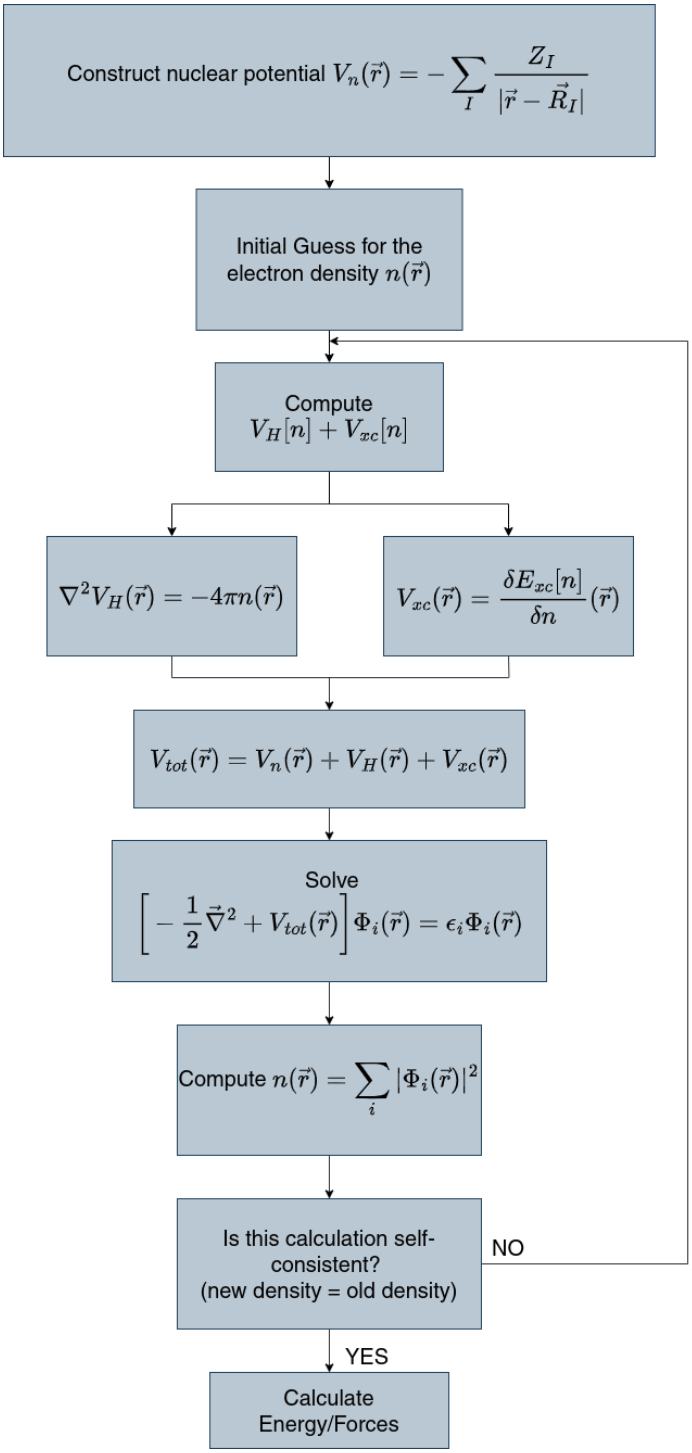

Figure 2.2: Flowchart of a self-consistent field calculation to solve the Kohn-Sham Equations in order to obtain e.g. the ground state energy of a system. Since the equations are all linked to each other, it is necessary to start with a guess for the electron density and, if needed, adapt the guess until self-consistency is achieved.

Chapter 3

Polarization in Perovskites

According to classical theory, perovskites can either display ferroelectric or paraelectric behavior, depending on the temperature. The transition from one phase to the other can be described by Landau theory. Some perovskite structures, however, exhibit a phase that deviates from the classical behavior. This phase is called quantum paraelectricity, in which the transition from paraelectricity to ferroelectricity is suppressed by quantum fluctuations. This chapter provides an outline of the three different phases and the Landau theory.

3.1 Ferroelectricity (FE) and Paraelectricity (PE)

Ferroelectrics are materials with an electric dipole moment that leads to a spontaneous electric polarization without having an external field present [17]. However, if an external field is present, the polarization can be inverted. For ferroelectricity to occur, a polar axis must exist [18]. Thus the crystal structure can't possess an inversion center, which means that the atoms with different charges must therefore be off-centered relative to each other.
The prefix "ferro" (=iron) refers to ferroelectricity being the counterpart of ferromagnetism, where, in contrast to ferroelectricity, there is not an asymmetry in charge but an asymmetry in spin. The prefix does not imply a connection to iron. Ferroelectricity was discovered in 1921 by J. Valasek, who conducted experiments on Rochelle salt (potassium sodium tartrate) and found that the salt remained spontaneously polarized after the external electric field was removed. This behavior, the so-called hysteresis curve, is shown in figure 3.1.
Paraelectric materials, on the other hand, exhibit dielectric polarization when an electric field is applied and lose this polarization when the field is removed [19]. This nonlinear relationship between electric fields and polarization is also shown in figure 3.1.

3.1.1 Transition from a FE phase to a PE phase

Ferroelectrics exhibit a temperature-dependent anomaly in their dielectric behavior, which is attributed to the phase transition [20]: when a ferroelectric crystal is heated, its polarization disappears above the critical Curie temperature and the crystal becomes a paraelectric, which does not have permanently parallel aligned electric dipoles

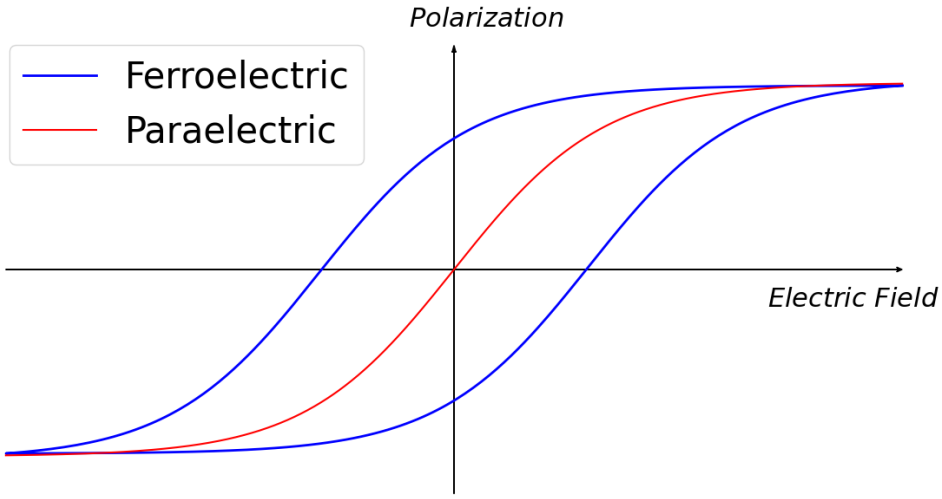

Figure 3.1: Polarization of a ferroelectric (paraelectric) material under the influence of an external electric field in blue (red). For the ferroelectric material, a hysteresis curve shows a finite polarization at zero electric field, whereas the paraelectric material exhibits finite polarization only with a finite electric field.

[21]. Paraelectrics have a statistical dielectric constant ϵ, which can be defined by the Curie-Weiss law as [21]

$$\epsilon(T) = \frac{C}{T - \Theta}\,.$$

Here, C describes a material-dependent constant, T represents the temperature, and Θ is the paraelectric Curie temperature. A high dielectric constant is therefore present at temperatures in the immediate vicinity of the Curie temperature. This is because even small changes in the electric field in this range lead to a significant displacement polarization of the crystal. These changes are on the order of 10^5 F/m [22]. In an idealized experiment, the dielectric constant would be infinite at the Curie temperature.
The transition of a perovskite from a paraelectric to a ferroelectric structure can be described in such a way that the central cation undergoes a permanent small change in its position so that it assumes an 'off-center' position relative to the surrounding oxygen anions [23]. As a result, the octahedral symmetry is broken and the net dipole moment is increased in proportion to the displacement of the titanium cation.
The difference between the two polarizing states in perovskite crystal structures of the form ABO_3 is illustrated as a schematic sketch in figure 3.2: the left-hand crystal is in a paraelectric phase, with its temperature being above the Curie temperature. The B-ion (orange) is in the center of the crystal and there is no polarization. The crystal structure on the right side is in a ferroelectric phase with a temperature below the Curie temperature. The central B-ion has moved away from its central position, which leads to a polarization of the crystal. From a microscopic point of view, the transition to ferroelectricity can be explained by the fact that the relative size of the A-cation prevents ideal nesting of the ions and since the distance of the B-cation to

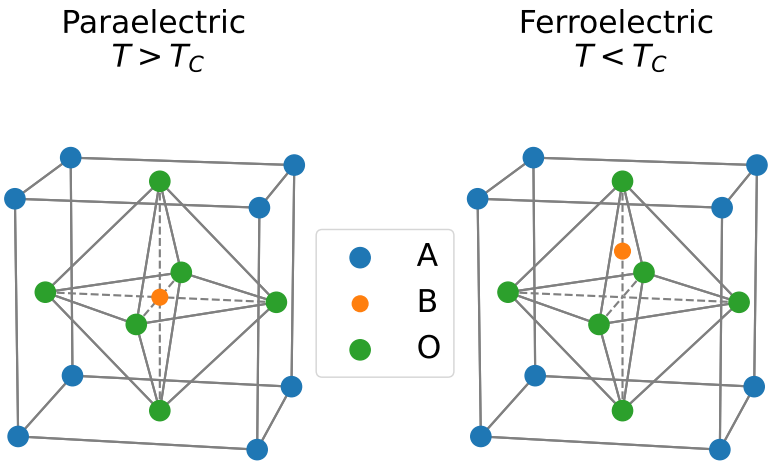

Figure 3.2: Schematic sketch of cubic ABO_3 perovskite structure in the symmetric paraelectric phase (left) and the ferroelectric phase (right), in which the central atom has moved away from its centered position, leading to polarization.

the oxygen is very large, it is likely that the B-cation leaves its centered position to get closer to one of the oxygen ions, which leads to the symmetry breaking [23].

3.1.2 Landau Theory

The theory of the phase transition of a material from its paraelectric to its ferroelectric state can be described using Landau theory. In general, there are two types of phase transition: first-order phase transitions, where the first derivative of the potential becomes discontinuous, and second-order phase transitions, where the second derivative of the potential becomes discontinuous [24]. The latter is also known as a continuous phase transition, as the state of the system changes continuously. For phase transitions in ferroelectrics, the second type is considered.
During a phase transitions, the symmetry of the system changes, as well as its properties. To describe a non-symmetric system through its state variables, an additional variable called the order parameter ψ, must be introduced, which describes the ordered state of a system. The order parameter can take its form through e.g. polarization. To describe the phase transition, the free energy $\mathcal{F}$, which is dependent on the order parameter as well as the temperature T, is considered. At the critical point the free energy $\mathcal{F}(T, \psi)$ has a minimum. It is assumed that the order parameter takes very small values near the transition, so $\mathcal{F}(T, \psi)$ can be expanded via Taylor expansion in powers of ψ. This results in [25]

$$\mathcal{F}(T, \psi) = F_0 + a(T)\psi^2 + \frac{b(T)}{2}\psi^4 \,.$$

This expansion was only developed up to the fourth order, as ψ should be small for $T \approx T_c$ with the critical Curie temperature T_c. The odd terms were neglected as the system should obey the symmetry $\mathcal{F}(T, \psi) = \mathcal{F}(T, -\psi)$. The expansion coefficients a and b are given by $a(T) \propto a_0(T - T_c)$ and $b \approx b_0 > 0$ [26]. The change from an ordered to a non-ordered state can be seen by the change of sign of a: if the temperature is

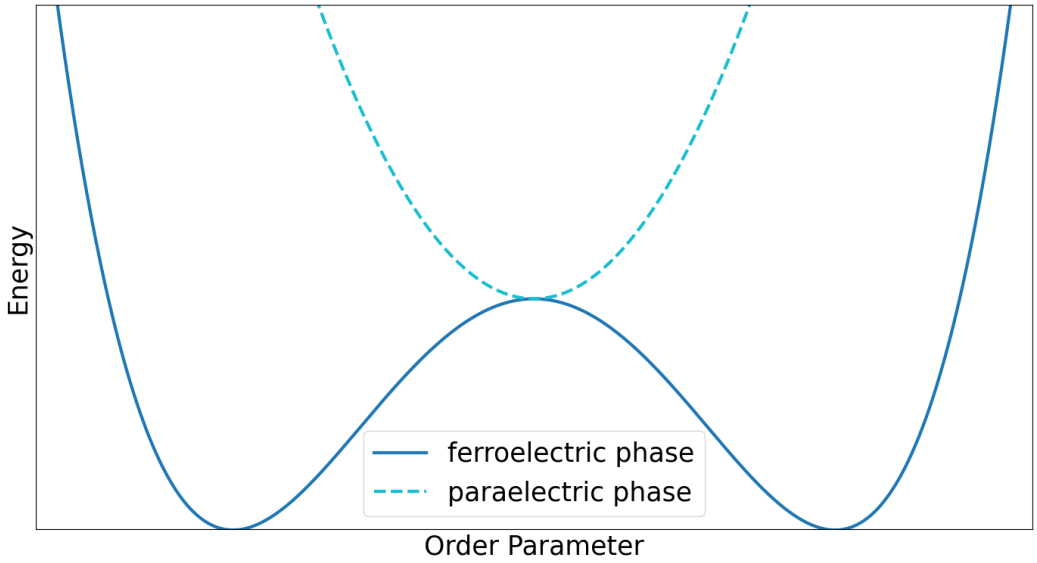

Figure 3.3: Sketch of the Landau free energy $\mathcal{F}$ as a function of the order parameter ψ. The double well potential (dark-blue line) represents the ferroelectric phase, whereas the parabola (light-blue dashed line) indicates a paraelectric phase.

above the Curie temperature, a is bigger than zero. At the phase transition, where the temperature reaches the critical temperature T_c, a is equal to zero, and at low temperature phases with the temperature being lower than the Curie temperature, a is smaller than zero.
The sketch of the graphical progression of the free energy is shown in figure 3.3. The dark blue line indicates the progression of the order parameter for the low-temperature phase. In this case, the order parameter has two minima, which results in the double-well shape of the potential. This low-temperature phase is referred to as 'ferroelectric'. Both minima of the potential represent a stable state of the system, which are both oppositely polarized, when imagining the order parameter as polarization. The light blue dashed curve indicates the behavior of the order parameter for the high-temperature phase, where the graph has a parabolic form. This phase is called 'paraelectric.'

3.2 Quantum Paraelectricity (QPE)

In addition to paraelectricity, which has no stable polarized state, and ferroelectricity, which has two stable polarized states, there exists a third state: quantum paraelectricity. In this case, the material is on the verge of becoming ferroelectric, but this transition is suppressed by quantum fluctuations between the two stable polarized states of the system, so the material remains paraelectric.

Finding the ground state energy via solution of the one particle Schrödinger equation

As a quantum mechanical description is needed, the Schrödinger equation is used to draw conclusions as to whether a crystal is a quantum paraelectric material.

To do this, the crystal structure, which consists of several atoms, is described using a one-dimensional single-particle structure. This is justified because typically only one phonon mode exists, which causes polarization in the structure. This mode is characterized by its frequency, for which eigenvectors of the dimension $3N_A$, where N_A is the number of atoms, can be calculated. But since this calculation is carried out only at Γ point, all unit cells will be displaced in the same way. This means that only one parameter, in this case the displacement along the eigenvectors, is relevant to describe the polarization. This results in a Schrödinger equation of the form [1]

$$\left(\frac{-\hbar^2}{2m}\frac{\mathrm{d}^2}{\mathrm{d}\xi^2} + \tilde{V}(\xi)\right)\tilde{\Psi}(\xi) = E\tilde{\Psi}(\xi)\,.$$

Here m describes the mass of the ions, ξ the ion displacement, $\tilde{V}$ the potential, $\tilde{\Psi}$ the wave function and E the energy eigenvalues. However, since neither the mass nor the displacement of a phonon are very well defined in solid state physics, the displacement is replaced by mass-weighted coordinates, which combine the mass and the displacement into one variable, which are defined via $q = \sqrt{m}\xi$ [1]. The mass weighted Schrödinger equation is thus given by

$$\left(\frac{-\hbar^2}{2}\frac{\mathrm{d}^2}{\mathrm{d}q^2} + V(q)\right)\psi(q) = E\psi(q)\,. \tag{3.1}$$

This derivation of this one-particle Schrödinger equation is based on a method from T. Esswein and N. Spaldin, who used eq. 3.1 to investigate quantum paraelectricity in perovskites [1]. The transition from $\tilde{\Psi}$ to ψ and $\tilde{V}$ to V indicates the different wave functions and potentials due to the transition.

Construction of a potential

A potential V now has to be constructed that represents the crystal structure as a function of the displacement ξ. The potential has to obey the symmetry $V(\xi) = V(-\xi)$. The Taylor expansion of such a potential leads to

$$V(\xi) \approx 0 + \frac{\mathrm{d}}{\mathrm{d}\xi}V\bigg|_{\xi=0}\xi + \frac{1}{2}\underbrace{\frac{\mathrm{d}^2}{\mathrm{d}\xi^2}V\bigg|_{\xi=0}}_{a}\xi^2 + \ldots \quad \approx \frac{1}{2}a\xi^2\,.$$

Since only small displacements are relevant and terms corresponding to uneven orders of ξ must vanish, the potential can be approximated harmonically. This leads to $a = \omega^2 m$ with the frequency ω and

$$V(\xi) = \frac{1}{2}\omega^2\underbrace{m\xi^2}_{q^2} = \frac{1}{2}\omega^2 q^2\,. \tag{3.2}$$

If the phonon frequencies at Γ point are calculated for a material and $\omega^2 > 0$ applies, meaning no instabilities of the structure, then the potential is given by the harmonic potential from eq. (3.2).
If, on the other hand, $\omega^2 < 0$ applies, indicating an unstable structure, then the parabola, which now opens downwards, leads to a diverging ground state energy. The

harmonic approximation is no longer sufficient. In this case the fourth-order term of the Taylor expansion has to be taken into account, which leads to

$$V(q) \approx \frac{\omega^2}{2} q^2 + cq^4 + a\,,$$

where a, c are parameters to be determined. Assume that the double well has its minima at σ, than the first derivative results in

$$\left.\frac{\mathrm{d}V(q)}{\mathrm{d}q}\right|_{q=\sigma} = \left.(\omega^2 q + 4cq^3)\right|_{q=\sigma} \Leftrightarrow \omega^2\sigma + 4c\sigma^3 = 0\,.$$

From this follows a value for c of $c = -\frac{\omega^2}{4\sigma^2}$.
In order to shift the potential, so that the minima of the potential are located at zero energy, the condition of $V(\sigma) = 0$ is used. This leads to

$$-\frac{\omega^2}{4a^2}\sigma^4 + \frac{\omega^2}{2}\sigma^2 + a = 0 \Leftrightarrow a = -\frac{\omega^2}{4}\sigma^2\,.$$

When defining the potential height as $V_0 := -\frac{\omega^2}{4}\sigma^2$, the potential can be written as

$$V(q) = V_0\left(\frac{q^4}{\sigma^4} - 2\frac{q^2}{\sigma^2} + 1\right). \tag{3.3}$$

This potential is used in the method of T. Esswein and N. Spaldin [1] and can be seen in figure 3.4, where the blue dashed line represents the half-width σ and the orange line shows the potential height V_0. σ can be determined from

$$\sigma^2 = -\frac{4V_0}{\omega^2}\,. \tag{3.4}$$

As in the Landau theory, the paraelectric phase is characterized by a parabola, which results from the lack of instabilities in the crystal structure, shown in the presence of only positive frequencies for the phonon-calculation at Γ-point. In contrast are the quantum paraelectric as well as the ferroelectric phase, where these instabilities do occur. This is the reason why both phases can be described by the double-well potential given in eq. (3.3). In order to view the problem through a quantum mechanical lense, the crystal structure is approximated as one particle, for which the ground state energy and its probability density can be evaluated. The probability density must be symmetrical, so there are two possibilities for its form: on the one hand, it can be localized in the minima. On the other hand, the ground state energy could be delocalized across both minima. This can be seen in fig. 3.5. The ferroelectric state can be explained classically: in a double- well potential, the particle can either be in the left or right minimum. When applying a quantum mechanical description, this means, that the probability density (green line) is localized in one of the minima of the double well.
For the quantum paraelectric state however, there occurs a delocalization across the potential. This can be explained through the quantum character of the nuclei, which means that tunneling possibilities exists, leading to a deviation from the localized ground state.

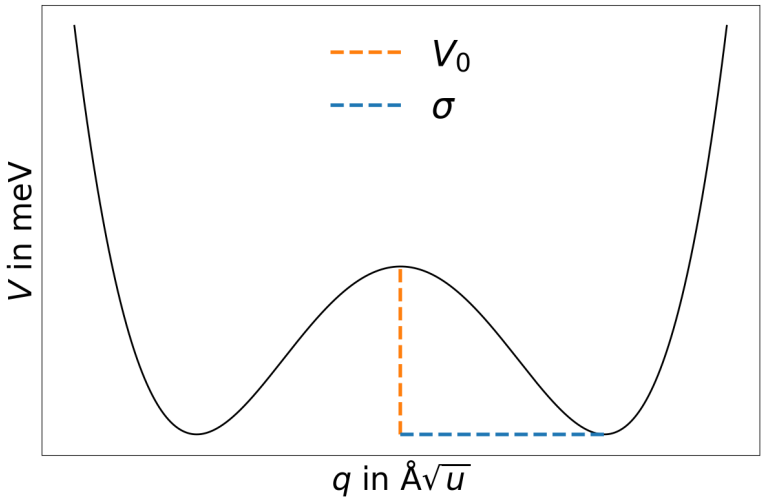

Figure 3.4: Double Well Potential. V_0 describes the height of the double well and σ the distance from the maximum to one of the minima

In order to now determine whether a material is quantum paraelectric, a double- well potential, like in eq. (3.3), has to be constructed, for which the Schrödinger equation, given by eq. (3.1), has to be solved numerically. This can be done by using the "scipy.linalg" library [1] in python. If the results yield a delocalization of the ground state, the material can be assumed to be a quantum paraelectric one.

The transition in perovskites of the ABO_3 structure to a ferroelectric state at low temperatures can be explained because their polar transverse optical phonon mode softens, turning the material unstable [27]. Having a soft phonon means that its frequency approaches zero at the critical temperature [17]. The vibrational pattern of a polarizing phonon mode in a perovskite is depicted in fig. 3.6. The closer the material is to the critical temperature, the more the frequencies of the vibrations decrease, which leads to a polarization of the material. In the context of the double well potential, this means that the structure falls in one of the polarized states of the double well potential spontaneously, which in turn leads to a macroscopic polarization. In other materials, e.g. strontium titanate, this softening does not occur at very low temperatures. Its ferroelectric soft mode stabilizes and ferroelectric behavior does not appear [27]. This has been explained by quantum fluctuations between the two polarized states that prevent the formation of a macroscopic dipole, keeping the material in a paraelectric state. This behavior is called "quantum paraelectric".

[1] https://docs.scipy.org/doc/scipy/index.html

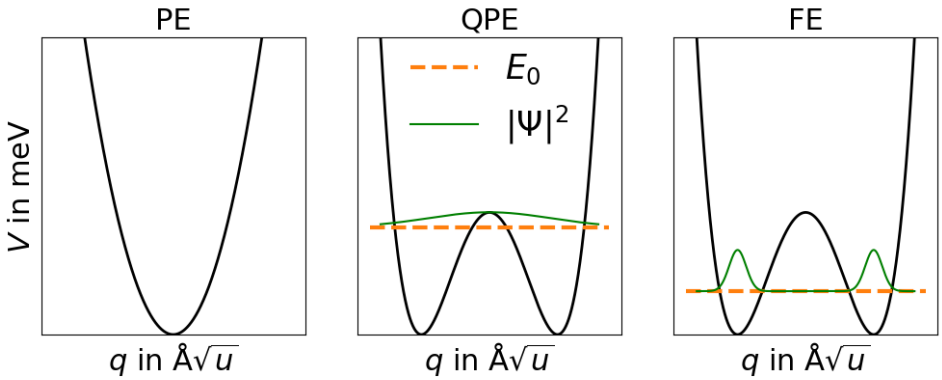

Figure 3.5: External parameters can be used to generate the transition from the ferroelectric state (FE) to the quantum paraelectric state (QPE) through to the paraelectric state (PE). For the PE phase, the potential still has the form of a parabola. For the QPE and the FE phase the potential is given by a double-well potential, with the difference, that the probability density (green line) of the ground state (with the ground state energy in orange) is clearly localized for the FE state, whereas for the QPE state, there exists a delocalization.

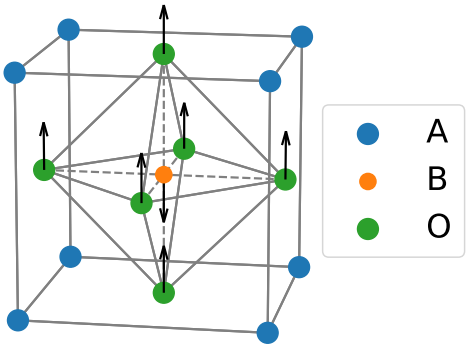

Figure 3.6: Schematic sketch of the vibrational pattern of a polarizing phonon mode in a perovskite of the ABO_3 structure. The closer the material is to the critical temperature, the more the frequency of the vibrations decrease, leading to a polarized structure.

Chapter 4

Computation of QPE

Strontium titanate is one of the best studied perovskites at the moment. It is a very interesting material, because it displays quantum paraelectric behavior at low temperatures. One method to investigate this property, using DFT and a one-particle Schrödinger equation, was suggested by T. Esswein and N. Spaldin [25], who applied this method to different single perovskites strontium titanate among others. In this chapter this method will be introduced and the results from the calculations, verifying the quantum paraelectric character of strontium titanate, will be presented and compared to the reference values of [25].

4.1 Strontium Titanate

Strontium titanate (STO), see figure 1.1, is one of the best-researched perovskites. It consists of a cubic structure, for which the unit cell is composed of a strontium cation, a titanium cation and three oxygen anions. As for all perovskites, the anions form an octahedral structure. The band structure is shown in figure 4.1. There is a band gap between the conduction and valence bands, which means that strontium titanate is a semiconductor. The experimentally measured indirect bandgap is 3.25 eV and the direct bandgap is 3.75 eV [28]. However, the band structure calculated with Quantum ESPRESSO from figure 4.1 provides a direct band gap at the Γ point of ≈ 2.2 eV. This could be due to the fact that the experiments are usually carried out at room temperature, while the Quantum ESPRESSO calculations take place at 0 K.

The phonon dispersion of the symmetrical structure of a $2 \times 2 \times 1$ $SrTiO_3$-supercell is shown in figure 4.2. At the Γ-point, modes converge at zero frequency. These are the acoustic phonon modes, where the atoms move coherently out of their equilibrium position. The phonon modes, which have a non-zero frequency without any divergence, are the optical phonons, where the atoms move out of phase. At the Γ point, a lot of negative frequencies occur. These indicate the instability of the structure.

In the following, the quantum paraelectric character of strontium titanate will be investigated.

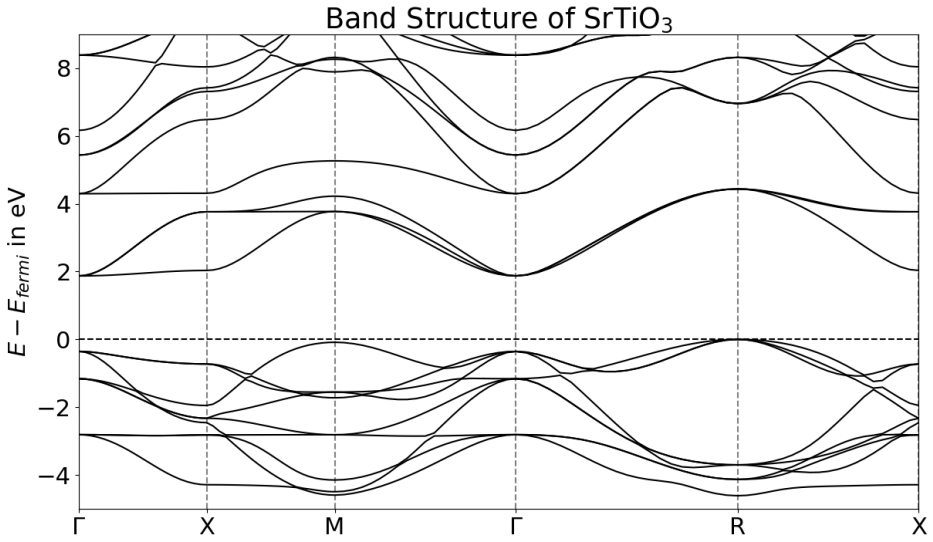

Figure 4.1: Band structure of $SrTiO_3$ with a direct bandgap of 2.2eV, thus making $SrTiO_3$ a semiconductor.

4.2 Method of Esswein/Spaldin

For the replication of the quantum paraelectric character of strontium titanate, Quantum ESPRESSO is used to conduct the relevant calculations to construct a double-well potential, given by eq. 3.3. With this potential the Schrödinger equation, given by eq. 3.1, can be solved and the probability density of the ground state can be obtained. However, since all Quantum ESPRESSO calculations take place at 0 K, Landau theory cannot be applied directly. A double-well potential is now assumed as the starting point for the calculation, in which a highly symmetrical crystal structure is located at the maximum of the potential at zero displacement. A relaxation calculation, which results in slightly different atomic positions and cell parameters, brings the crystal structure into a relaxed state. A self-consistent-field (SCF) calculation and a phonon calculation are performed. This, on one hand, provides the energy of the highly symmetric cubic structure E_{sym} and, on the other hand, supplies the eigenvectors that correspond to frequencies of the phonon modes.
The phonon calculation is only carried out at the Γ point in the Brillouin zone, since the Γ point is the most important point for a finite polarization of the crystal due to the spatial independence of the vibration: in a harmonic approximation, the time dependant displacement $\vec{y}(t)$ of the atom l at location $\vec{r}_l$ can be describe through plane waves, as a result it follows [29]

$$\vec{y}_{l,q,m}(t) = \vec{Y}_{l,m}(q) e^{i\vec{r}_l \cdot \vec{k}} e^{-i\omega_m t} \,,$$

where k is the wave vector of the considered phonon and ω_m and $\vec{Y}_{l,m}$ its corresponding frequency and eigenvector, obtained from the eigenvalue problem of the dynamical matrix. $\vec{Y}_{l,m}(q)$ states in which direction of the atom l is shifted through a phonon with wave vector q and frequency ω_m. Therefore the displacement at Γ point is no longer dependant on the location.
These eigenvectors are calculated through the eigenvalue problem

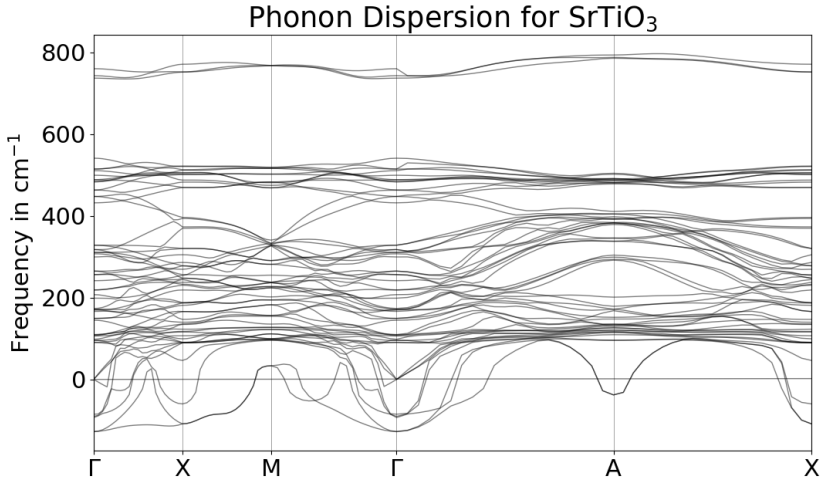

Figure 4.2: Phonon dispersion for the $2 \times 2 \times 1$ supercell of $SrTiO_3$. A lot of negative frequencies occur at Γ point, indicating a stability of the system.

$\mathbf{D}_l(q)\vec{Y}_{l,m}(q) = \omega^2\vec{Y}_{l,m}(q)$, where $\mathbf{D}_l(q)$ is the dynamical matrix.
If the solution of the dynamical matrix results in imaginary frequencies, it means that the system is in an unstable state. Since Quantum ESPRESSO can only depict the real parts of calculation results, the imaginary frequencies appear as negative ones in the output, because the imaginary frequencies are mapped onto the negative axis of the real part.
The atomic structure is now shifted along these eigenvectors that correspond to negative frequencies, meaning $\omega_m^2 < 0$. The change of position of an atom l at the Γ point can be calculated via

$$\vec{r}_l \to \vec{r}_l + \xi \sum_{\substack{m \\ \omega_m^2<0}} \vec{Y}_{l,m}(\Gamma)\,. \tag{4.1}$$

In this case ξ is the weighted factor with which all atoms will be displaced. Because there are more than one imaginary frequencies, all of of them will be considered for the displacement.
The quantum paraelectric phase results from quantum fluctuations between the two polarized states. Since it is now possible to specify the polarized state through a value for ξ (see eq. (4.1)), the whole structure can be viewed as one particle, whose system has the displacement ξ. This displacement can be interpreted as the "particle" being pushed towards either the left or right side of the potential. Now the structure is relaxed again, which leads to the "particle" falling into one of the two minima and another SCF- and phonon calculation is carried out (again only at the Γ-point). This results in the energy E_{displ} of the structure at the minimum. If the particle is now in one of these minima, which indicates a stable state, the phonon frequencies should no longer be negative.
The procedure, as well as the Schrödinger equation and the equation for the double-well potential, are based on "Ferroelectric, quantum paraelectric, or paraelectric? Calculating the evolution from $BaTiO_3$ to $SrTiO_3$ to $KTaO_3$ using a single-particle

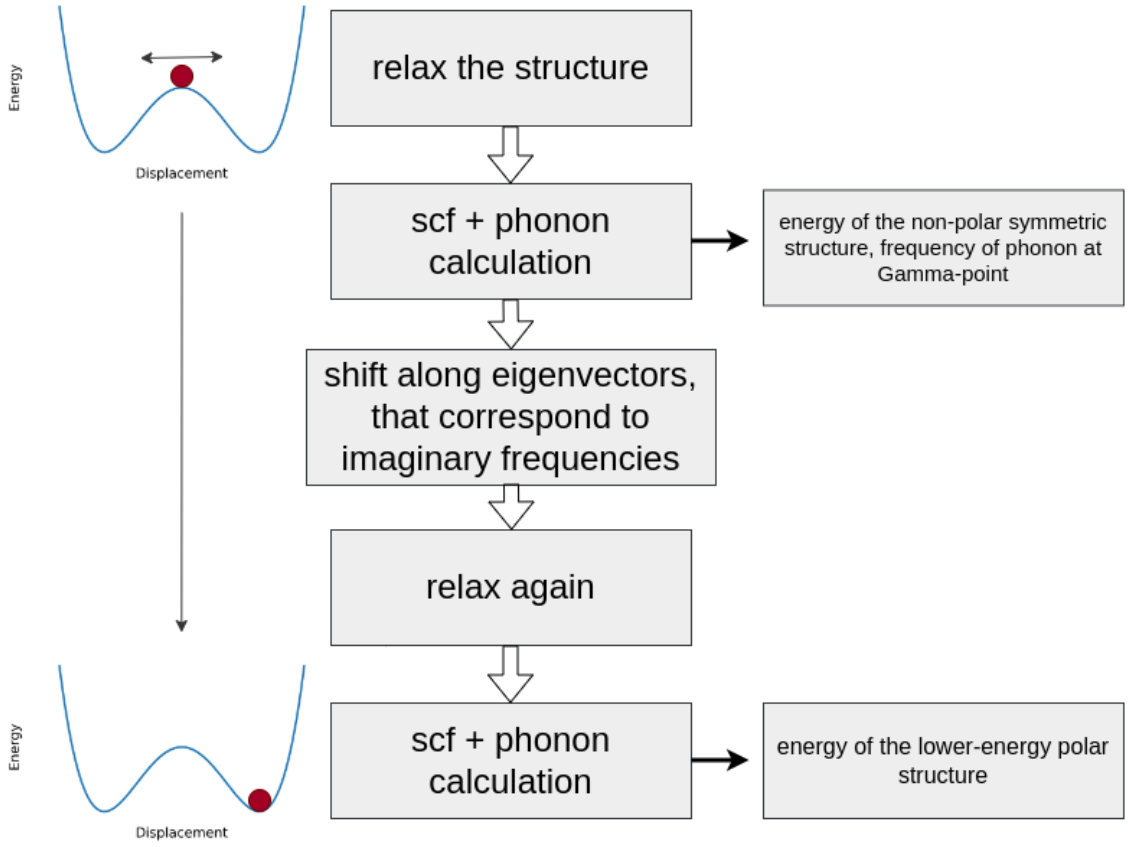

Figure 4.3: Calculation steps with Quantum ESPRESSO to reproduce that STO is a quantum paraelectic material.

quantum mechanical description of the ions" by Tobias Esswein and Nicola Spaldin, where these calculations are performed for different perovskites. The individual calculation steps are illustrated in figure 4.3. The potential barrier height can be calculated through the energy difference of the energy of the initial structure E_{sym} and the energy of the distorted structure E_{displ}. The half-width σ can be obtained from eq. 3.4. With those two values it is possible to construct a double- well potential, using eq. 3.3. For this potential the Schrödinger equation (see eq. 3.1) can be solved, thus determining the probability density of the ground state.

4.3 Comparison with the Results of Esswein/Spaldin

4.3.1 Computational Details

For the calculation of strontium titanate with Quantum ESPRESSO, a cubic $2 \times 2 \times 1$ supercell with 20 atoms was generated. A lattice constant of $7.4\,a_0$ (see A.1) was utilized. The convergence threshold for the total energy was set to $7.35 \times 10^{-8}\,\mathrm{Ry}$ and the threshold for the force to $3.89 \times 10^{-6}\,\mathrm{Ry}/a_0$. In addition, an $8 \times 8 \times 8$ k-point grid (see A.2) was used and the cut-off energy was set to $60\,\mathrm{Ry}$ (see A.3). For the calculation, "ultrasoft" pseudopotentials were chosen.

4.3.2 Results of the Schrödinger Equation

The calculation of strontium titanate with Quantum ESPRESSO resulted in an energy of $E_{sym} = -1148.0642\,\text{Ry}$ for the supercell of the highly symmetric crystal structure at the maximum at zero displacement and an energy of $E_{displ} = -1148.0657\,\text{Ry}$ for the supercell of the distorted final structure at the minimum. The potential height V_0 can now be calculated via $(E_{sym} - E_{displ})/4$. The denominator is set to four to obtain the value for a five-atom unit cell of strontium titanate. This results in $V_0 = 0.000\,383\,85\,\text{Ry}$, which converts to 5.22 meV, see table 4.1. The frequency at the Γ point was 5.6954 THz. Thus, with eq. (3.4) a value for σ of $0.623\,\text{Å}\sqrt{\text{u}}$ could be calculated. The conversion of σ into units of $\text{Å}\sqrt{\text{u}}$ was performed in order to compare the calculated results with the reference values from the paper by T. Esswein and N. Spaldin "Ferroelectric, Quantum Paraelectric, or Paraelectric?" [25].
Since the mass of the structure must be taken into account in the conversion to $\text{Å}\sqrt{\text{u}}$, the variant, proposed in the paper, was chosen using the mass of the lightest atom, in this case that of the oxygen atom with an atomic mass of 15.999 u.
The comparison of the calculated potential with the reference potential from [1] is shown in figure 4.4. The paper calculated a potential height of $\tilde{V}_0 = 5.74\,\text{meV}$ and a σ value of $\tilde{\sigma} = 0.571\,\text{Å}\sqrt{\text{u}}$. This means that the deviation of the potential height from the reference value is $\approx 9\%$, while the deviation of the σ value from the reference value is also $\approx 9\%$. Since the difference between the two results in a very small order of magnitude due to the high energies, the deviation is not too relevant. This also becomes clear in figure 4.4: at the relevant points, from one minimum to the other, the calculated potential approximately matches the reference potential. The deviation could stem from possible different input parameters for the density functional calculations.

The Schrödinger equation could now be solved numerically using this potential.

	V_0 in meV	σ in $\text{Å}\sqrt{\text{u}}$	$E_1 - E_0$ in meV	$E_0 - V_0$ in meV
own values	5.22	0.623	9.10	1.02
values from [1]	5.74	0.571	10.02	1.12

Table 4.1: Calculated values compared to values from the paper [1]. The calculated values deviated by 9% from the reference values. The difference could stem from using different input parameters for the Quantum ESPRESSO calculations.

The result is shown in figure 4.5. The ground state energy is $E_0 = 6.24\,\text{meV}$ and the energy of the first excited state is $E_1 = 15.34\,\text{meV}$. The probability density of the ground state (blue) is delocalized over both minima and has its maximum at zero displacement. With the potential having the form of a double well, combined with this delocalization, it can be concluded that strontium titanate is indeed a quantum paraelectric material.
Comparing the difference between the two states $E_1 - E_0$ gives an energy difference of 9.10 meV, which in turn differs by $\approx 9\%$ from the energy difference of the states in the reference paper of 10.02 meV. The difference of the potential barrier to the ground state $E_0 - V_0$ with 1.02 meV from the self-calculated solution and 1.12 meV from the reference value also deviates by the same percentage. The calculated values compared to the values from [1] are shown in table 4.1.

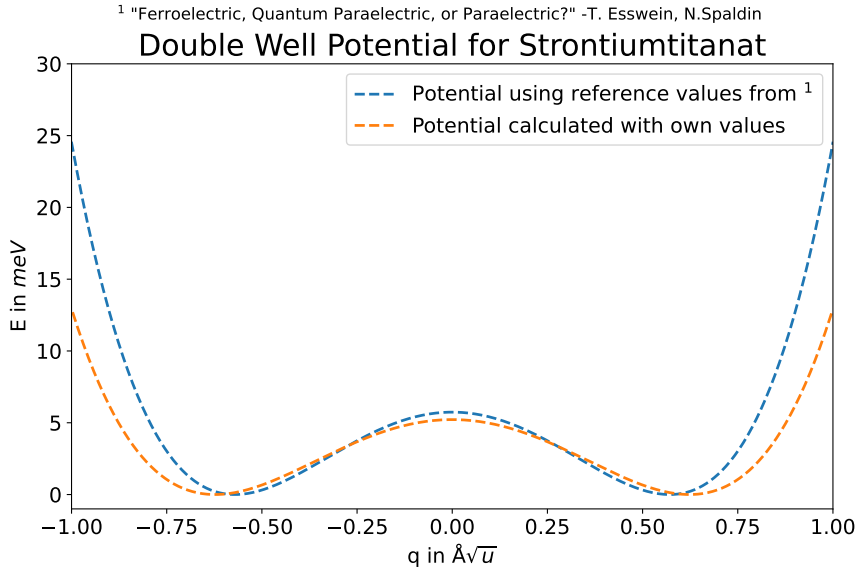

Figure 4.4: Double-well potential for $SrTiO_3$ with the self calculated values (orange) and the reference values (blue) from [1]. The difference between the potentials increases towards the edges, but in the relevant sections, from one minimum to the other, the potentials approximately match: the calculated potential has a potential barrier of 5.22 meV, while the reference potential has a barrier of 5.74 meV. The reference σ value is 0.571 $\text{Å}\sqrt{\text{u}}$, while the calculated one is 0.623 $\text{Å}\sqrt{\text{u}}$.

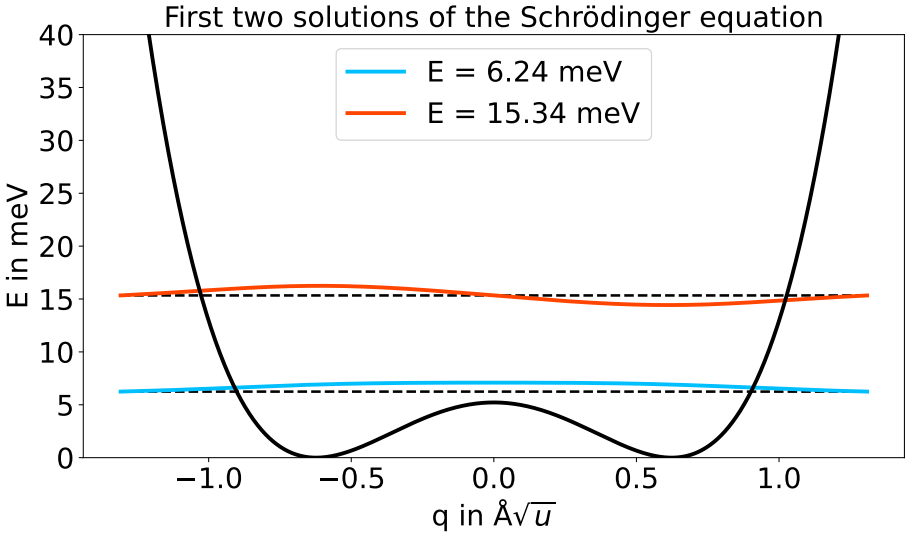

Figure 4.5: The eigenenergies and the eigenstates of the Schrödinger equation for $SrTiO_3$ with the ground state (blue) and the first excited state (red). The potential height is at 5.22 meV, which is in the vicinity of the energy of the first excited state at 6.24 meV. The ground state is non-degenerate and the energy of the first excited state is at 15.34 meV. Since the probability density of the ground state is delocalized over the potential and the potential has the form of a double well, it can be concluded that strontium titanate is a quantum paraelectric material.

In summary, it can be said that this method is suitable for determining whether a crystal structure is a quantum paraelectric one, since it was possible to reproduce the quantum paraelectric character of strontium titanate.

Chapter 5

QPE in Double Perovskites

In addition to simple perovskite structures, there exist double perovskites, which are composed of two individual simple perovskites. However, double perovskites are not as well-studied as single perovskites, making them an interesting subject to study. The quantum paraelectic character of a simple perovskite structure can be demonstrated using the method described in chapter 4.2. This chapter addresses the question of whether quantum paraelectricity, which has been found in the simple perovskite strontium titanate, can also be found in double perovskites.

5.1 Procedure and Computational Details

A total of 77 double perovskite are considered, which are listed in table A.1. All of those double-perovskites have the same electronic configuration as strontium titanate. For each of these crystal structures, the procedure presented in chapter 4.2 was carried out: a highly symmetric structure at zero displacement is first relaxed, a SCF- and phonon calculation are carried out, the structure is shifted along the resulting eigenvectors corresponding to negative frequencies and the structure is relaxed again. For each double perovskite, a cubic structure with a total of 10 atoms was used to perform the calculation. The cutoff energy was set to 60 Ry (see fig. A.4, where the convergence test of the lattice constant for Sr_2CaWO_6 is shown), the convergence threshold for the energy was set to 1.0×10^{-7} Ry and the force convergence threshold to $1.0 \times 10^{-6}\,\mathrm{Ry}/a_0$. The calculation was performed on an $8 \times 8 \times 8$ k-point mesh (see fig. A.5 for Sr_2CaWO_6). The lattice constant was set to $11.17\,a_0$ (see fig. A.6 for Sr_2CaWO_6). Again "ultrasoft" pseudopotentials were used.

5.2 Results of the Schrödinger Equation

The energies calculated with Quantum ESPRESSO for the highly symmetrical structure at zero displacement, E_{sym}, the relaxed, distorted structure, E_{displ}, and the frequency ω at the Γ-point are shown in table A.1. Table A.1 also shows the potential barrier V_0, which results from the difference between the highly symmetrical and the relaxed structure, as well as the value of the half-width of the potential σ, which can be obtained from eq. (3.4). For the calculation of σ, as with strontium titanate, the mass of the lightest atom was used, which is also shown in table A.1.

Some calculated potential heights have a value of zero (e.g. Ba_2YVO_6), some have potential heights were so small, that they can be assumed to be zero (e.g. $Cs_2LiLaBr_6$, whose potential height was calculated to 1×10^{-8} Ry) and even some negative potential heights occurred (e.g. $Cs_2NaScCl_6$ with a potential height of -1.5×10^{-7} Ry). For all those double perovskites it is not possible to construct a double well potential, which is why these materials can already be assumed to be paraelectric. The potential of those materials, as explained in section 3.2, takes a parabolic form at zero displacement, since the lowest-energy state of the structure is already present in its non-polar form.
The reason for negative potential heights is, that one can imagine that the "particle" is initially at the minimum of the parabola and that the potential moves upwards a little as the structure is shifted along the negative eigenvectors. This shift along negative eigenvectors, which indicate instability of the structure, is due to numerical inaccuracies: negative frequencies actually exist for these materials, but since they are so small, they can be regarded as zero. However, since the calculation was executed using an automated code, it was not possible to discern those structures. The shift along the negative eigenvectors was carried out nonetheless and the calculation continued from this point on. In total 13 paraelectric materials could be found.
For the remaining 64 crystal structures, the Schrödinger equation, given by eq. (3.1), was solved numerically. The ground state energies E_0, the energies of the first excited states E_1 and the potential barriers V_0 are shown in table A.2. It is noticeable that there are significant fluctuations in the potential barriers: the lowest heights are in the range of ≈ 30 meV, as with Ba_2CaMoO_6 (see fig. 5.1), while the largest barriers is at ≈ 3500 meV for La_2CaZrO_6 (see fig. 5.2). For 62 of the 64 double perovskites, the ground state energy is clearly below the potential barrier and the probability density is localized in one of the two minima. This is also the case for Ba_2CaMoO_6 and La_2CaZrO_6. If the energy of the first excited state is also calculated, it can be seen that for 11 of the 62 crystal structures the ground state energy is not degenerate, meaning that the ground state energy differs from the one of the first excited state. These changes range from a difference from the first decimal point up to a difference in the fifth.
In conclusion 62 materials appear to be ferroelectric, and of those 11 double perovskites have a non-degenerate ground state.

5.2.1 Potential Quantum Paraelectrics

Of the 77 double perovskites examined, 2 materials were found that do not exhibit the typical ferroelectric or paraelectric character: Cs_2NaYCl_6 and Rb_2LiYCl_6.
Cs_2NaYCl_6 has a potential height of 0.3317 meV, so its potential height is very small, but the potential still displays a double-well. This is depicted in fig. 5.3. The ground state energy is 7.859 meV and the associated probability density (in blue) is delocalized over both minima. As with strontium titanate, the ground state is not degenerate: the energy of the first excited state is 28.713 meV. The double-well character and the shape of the probability density indicate quantum paraelectic behavior of this double perovskite.
The band structure is shown in figure 5.4. It can be seen that the crystal falls within

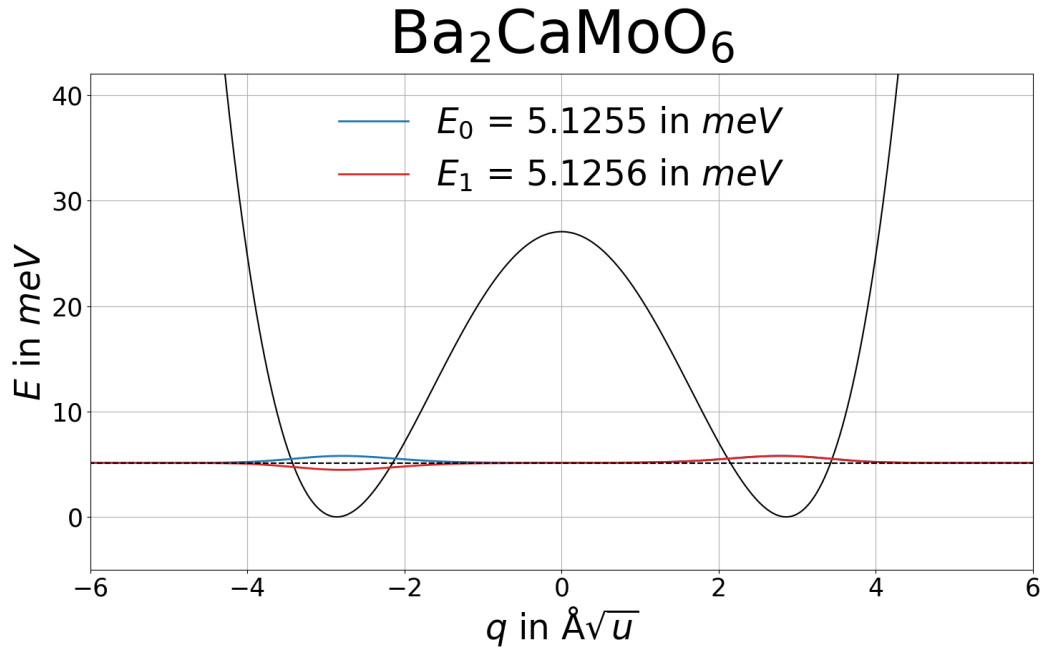

Figure 5.1: Energy and eigenstates of the degenerate ground state (blue, red) of Ba_2CaMoO_6, which has a potential barrier of $\approx 30\,\text{meV}$. This value of the potential heights was one of the smallest calculated.

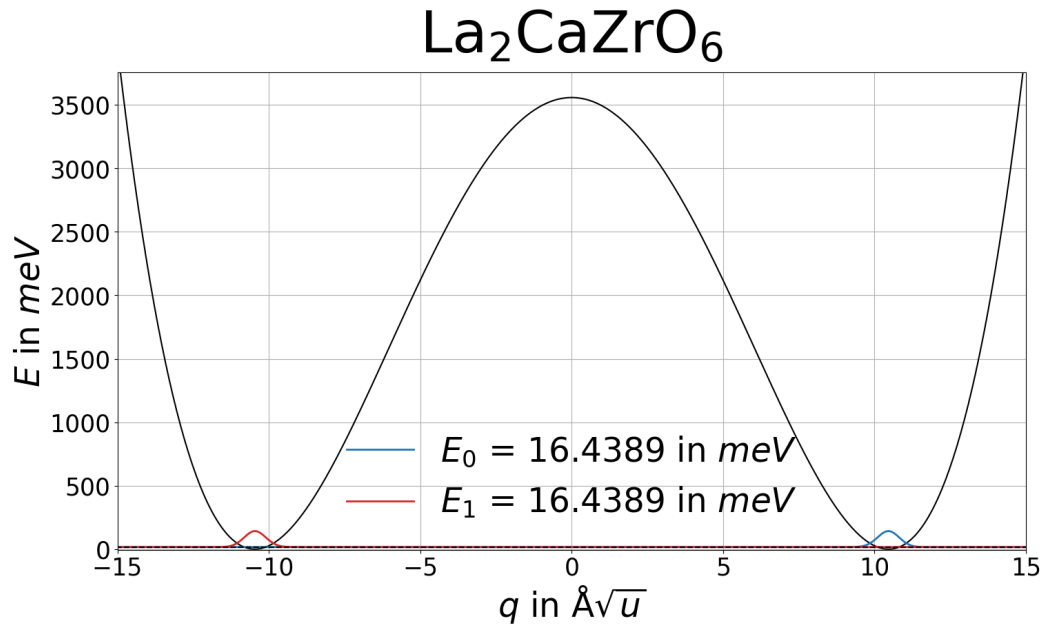

Figure 5.2: Energy and eigenstates of the degenerate ground state (blue, red) of La_2CaZrO_6, which has a potential barrier of $\approx 3500\,\text{meV}$. This was the biggest calculated potential barrier. Here the eigenstates had to be amplified by 100 in order to see their shapes.

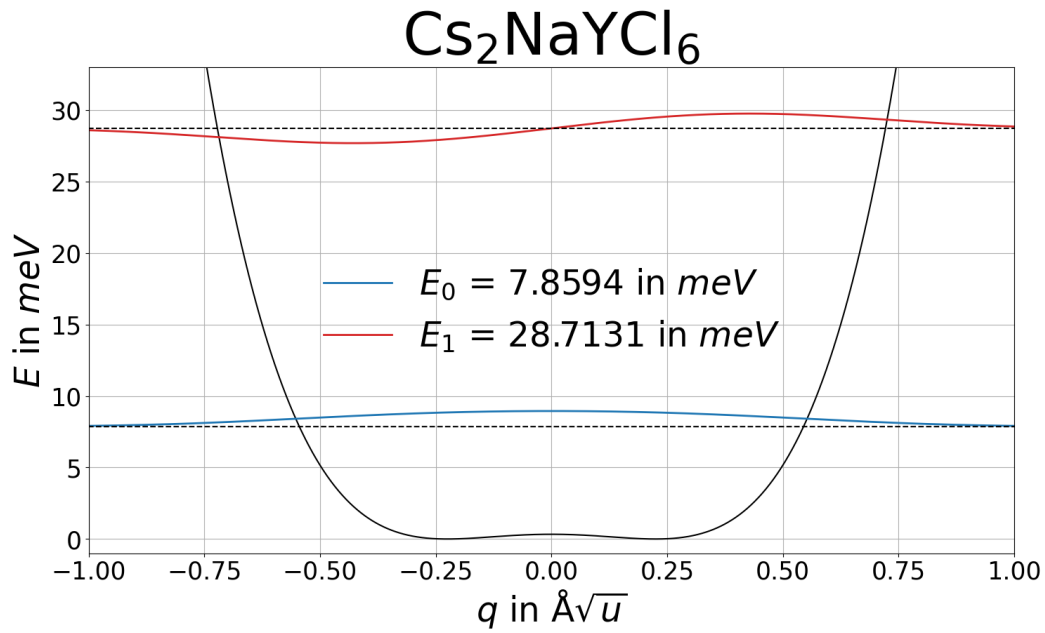

Figure 5.3: Potential of Cs_2NaYCl_6 with the first two solutions of the Schrödinger equation. The potential barrier is at 0.3317 meV, which is relatively small compared to the energy of the ground state at 7.859 meV. The ground state is non-degenerate and the energy of the first excited state is 28.713 meV. The ground state solution has a probability density (blue) that is delocalized over both minima, which together with the double well shape indicates quantum paraelectricity.

the semiconductors due to its band gap. The direct band gap can be estimated to be $\approx 2.6\,\text{eV}$ at the Γ point, which is of the same order of magnitude as the band gap determined with Quantum ESPRESSO at the Γ-point of strontium titanate with $\approx 2.2\,\text{eV}$.

The phonon dispersion of the highly symmetrical structure can be seen in figure 5.5. Just like with strontium titanate, the acoustic phonon modes converge at Γ point, whereas the optical ones do not. The negative frequencies indicate the instability of the structure.

The second double perovskite whose solutions of the Schrödinger equation together with its potential form deviates from those of ferroelectrics or paraelectrics is Rb_2LiYCl_6. Here the ground state energy is below the maximum of the double-well potential, shown in fig. 5.6. The probability density of the ground state (blue) is delocalized, but it is still possible to discern two maxima in the minima of the potential. The potential height is 15.8580 meV, which is above the ground state energy at 9.623 meV and that of the first excited state at 12.214 meV.

As with Cs_2NaYCl_6, the band structure, illustrated in graphic 5.7 shows that Rb_2LiYCl_6 is a semiconductor. Here the smallest band gap is at the Γ point with $\approx 3.5\,\text{eV}$. This is therefore of the same order of magnitude as the experimentally measured band gap of strontium titanate at 3.75 eV.

The phonon dispersion of Rb_2LiYCl_6, shown in figure 5.8, has similarities to that of Cs_2NaYCl_6: the acoustic frequencies converge at the Γ point and several negative frequencies exist due to the instability of the highly symmetrical structure.

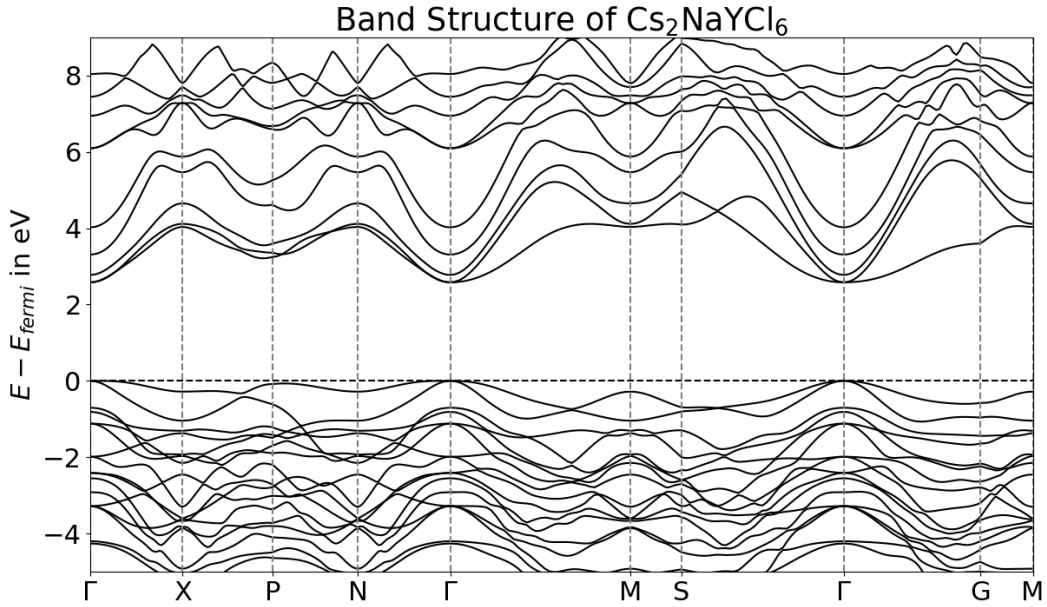

Figure 5.4: Band structure of Cs_2NaYCl_6. It can be seen from the band gap that Cs_2NaYCl_6 is a semiconductor.

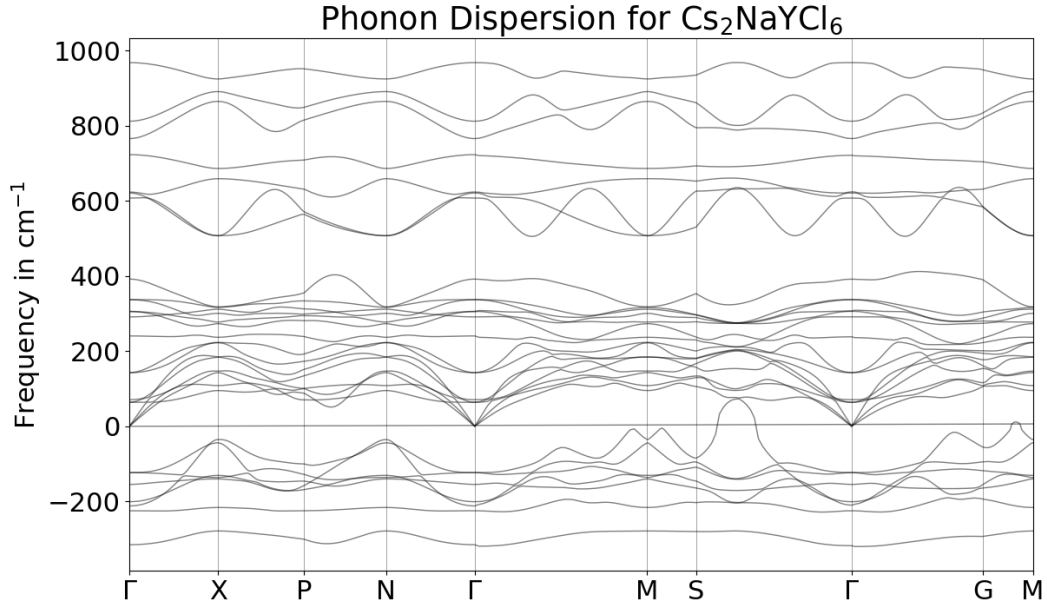

Figure 5.5: Phonon dispersion of the highly symmetrical structure of Cs_2NaYCl_6. A lot of negative frequencies can be found at Γ point, indicating a an instable structure.

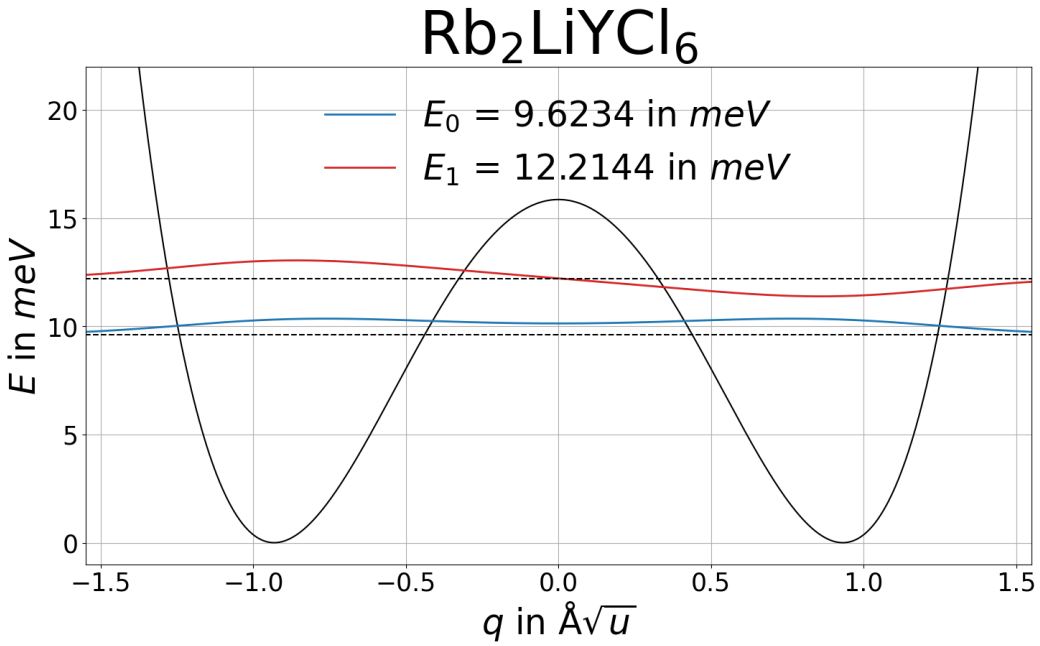

Figure 5.6: First two solutions of the Schrödinger equation of Rb_2LiYCl_6. The potential barrier height is, with a value of 15.8580 meV, higher than the energy of the groundstate (9.623 meV) and that of the first excited state (12.214 meV). The ground state has a probability density (blue) which is delocalized over both minima, but maxima can nevertheless be detected in the minima of the potential. However, with the double well shape and the delocalization, Rb_2LiYCl_6 falls under the quantum paraelectrics.

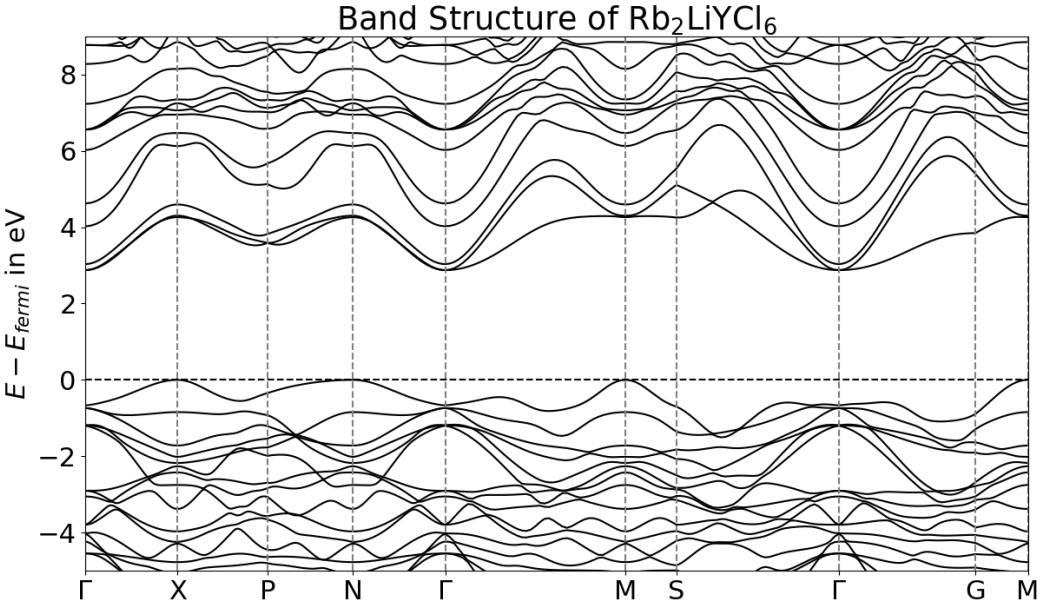

Figure 5.7: Band Structure of Rb_2LiYCl_6. The direct band gap here is ≈ 3.5 eV at the Γ point, making Rb_2LiYCl_6 a semiconductor.

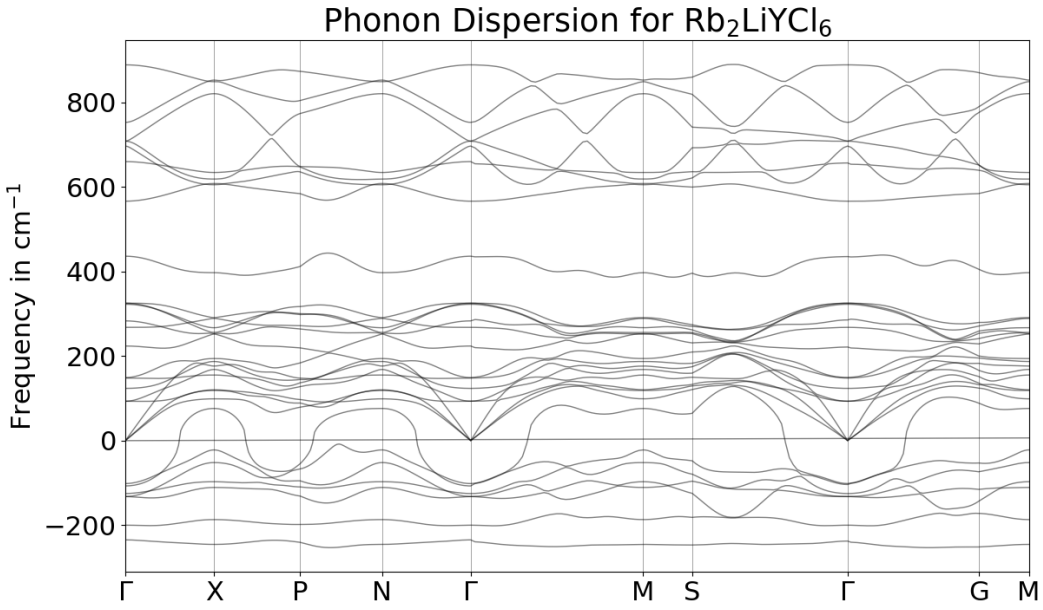

Figure 5.8: Phonon Dispersion of the highly symmetric structure of Rb_2LiYCl_6, displaying a similar phonon dispersion like Cs_2NaYCl_6 with many negative frequencies, which indicate the instability of the structure.

5.2.2 Correlations concerning the Potential Barrier Height

In order to find an explanation for the differences in the potential height discussed in section 5.2.1, a correlation between the ionic radii of the B- and B'- ions and the potential height V_0 was first investigated. As can be seen in figure 5.9, there is no correlation between the ionic radii of the B- and B'- ions and the potential height V_0. The ionic radii used are shown in table A.3.

After looking at the ionic radii of the B- and B' -ion directly, now the geometric factors, which are dependent on the ionic radii of the respective structures, mentioned in chapter 1, are taken into account. The tolerance factor t_s and the octahedral factor μ_s of the simple perovskites indicate the stability of perovskites (see figure 1.2). The tolerance factor is defined via

$$t_s = \frac{r_A + r_X}{\sqrt{2}(r_B + r_X)} \tag{5.1}$$

and the octahedral factor is given by

$$\mu_s = \frac{r_B}{r_X}\,, \tag{5.2}$$

where r_A, r_B, and r_X are the respective ionic radii of the ion [2]. This concept can also be applied to double perovskites of the form $A_2BB'X_6$. However, since there is a B- and a B'-ion, two factors must be defined for the octahedral structure: the average octahedral factor $\bar{\mu}$ and the octahedral mismatch $\Delta\mu$ with [2]

$$\bar{\mu} = \frac{(r_B + r_{B'})}{2r_X} \tag{5.3}$$

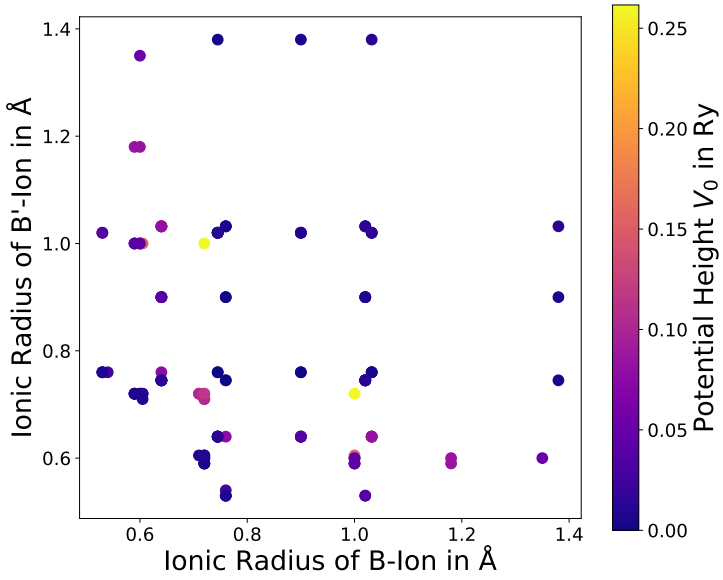

Figure 5.9: Ionic radii of the B and B' ions as a function of the potential height V_0. No correlation can be determined.

and

$$\Delta\mu = \frac{|r_B - r_{B'}|}{2r_X}\,. \tag{5.4}$$

The generalized tolerance factor t of the double perovskites is given by [2]

$$t = \frac{\left(\frac{r_A}{r_X} + 1\right)}{\sqrt{2(\bar{\mu}+1)^2 + \Delta\mu^2}}\,. \tag{5.5}$$

The ionic radii from table A.3 were again used for the calculation. All results for the geometric factors are depicted in table A.3 as well. For double perovskites, this set of geometric factors results in a "generalized stability region, (which is a) closed volume in the ($\bar{\mu}$,t,$\Delta\mu$) space." - M. Filip and F. Giustino, "The geometric blueprint of perovskites" [2].
The dependence of the potential height V_0 on the generalized tolerance factor t is shown in figure 5.10. The blue dots represent the ferroelectric materials. In the semi-logarithmic representation chosen here, a linear relationship can be recognized between the tolerance factor of the ferroelectrics and their potential height, which is given by $V_0(t) = \exp\{-21.1t + 15.59\}$. In order to display the paraelectric materials (in orange) in this plot, the absolute value of V_0 was used on the y-axis. It is noticeable that the paraelectrics have a higher tolerance factor compared to the ferroelectrics. This also seems reasonable, as a lower tolerance factor indicates a greater distortion of the structure and the deviation from the highly symmetrical cubic shape of the ferroelectrics is decisive for their polarization.
The red dot is strontium titanate as a reference value for a quantum paraelectric

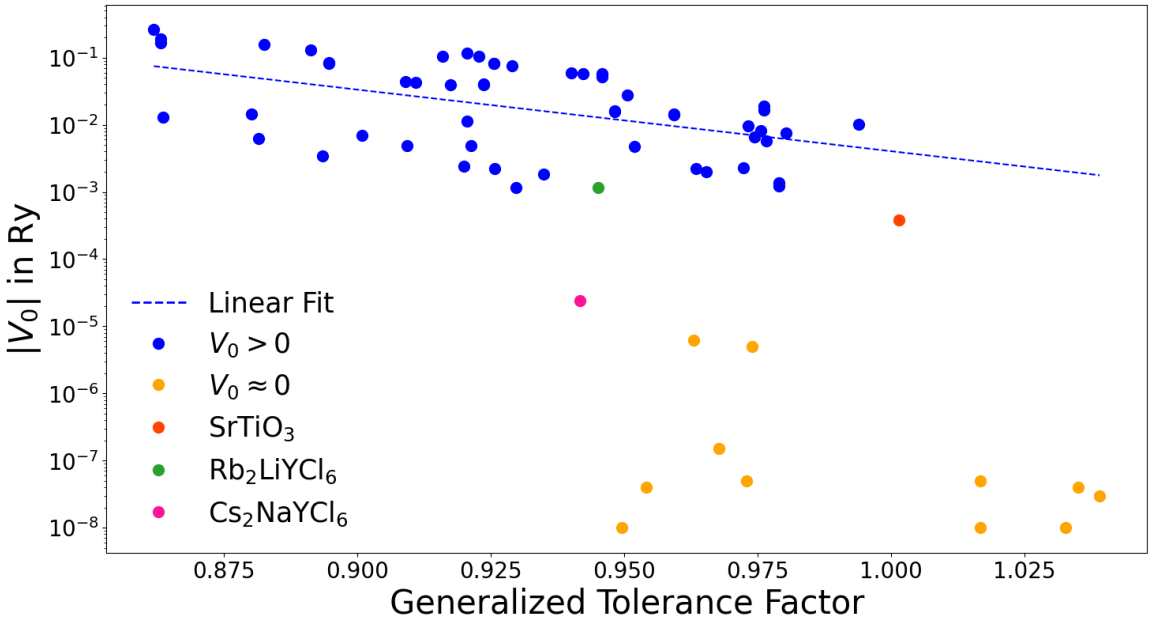

Figure 5.10: Absolute value of the potential height V_0 in semi-logarithmic representation as a function of the generalized tolerance factor t (see eq. 5.5). The orange dots represent the paraelectric materials that have a potential height of approximately zero. Compared to the other double perovskites, they have a comparatively high tolerance factor, indicating less distortions in the structure. The blue dots represent the ferroelectric materials, between which a linear relationship can be recognized in the semi-logarithmic representation. The red dot shows strontium titanate as a reference value for a quantum paraelectric material. The two materials that are possible quantum paraelectrics, Cs_2NaYCl_6 (pink) and Rb_2LiYCl_6 (green), lie in the vicinity of $SrTiO_3$.

material. This value was calculated using equation (5.1). It is easy to see that strontium titanate has a tolerance factor of approximately one due to its cubic structure. It is also noticeable that the two possible quantum paraelectrics, Cs_2NaYCl_6 (pink) and Rb_2LiYCl_6 (green), are close to the value of the potential height of strontium titanate and are located in the area between the ferroelectric and paraelectric materials. Cs_2NaYCl_6 is closer to the paraelectrics, while Rb_2LiYCl_6 is very near the to region of the ferroelectrics. This is also to be expected based on the solutions of the Schrödinger equation: the ground state energy of Cs_2NaYCl_6 has a higher value than the comparatively small potential height V_0. It is therefore much closer to the paraelectric structures than Rb_2LiYCl_6. Here, the ground state and the first excited state were close to, but still below the potential barrier. The probability density of the ground state did not have a clear maximum at zero displacement, but there were minimal tendencies towards a localization in one of the two potential minima. This solution is therefore much closer to those of the ferroelectrics.

In figure 5.11 the same situation as in figure 5.10 is shown again, with the difference that the ferroelectric materials are divided into those that have a non-degenerate ground state (purple), which means that the energy of the first excited state is different from the ground state energy, and those that have a degenerate ground state

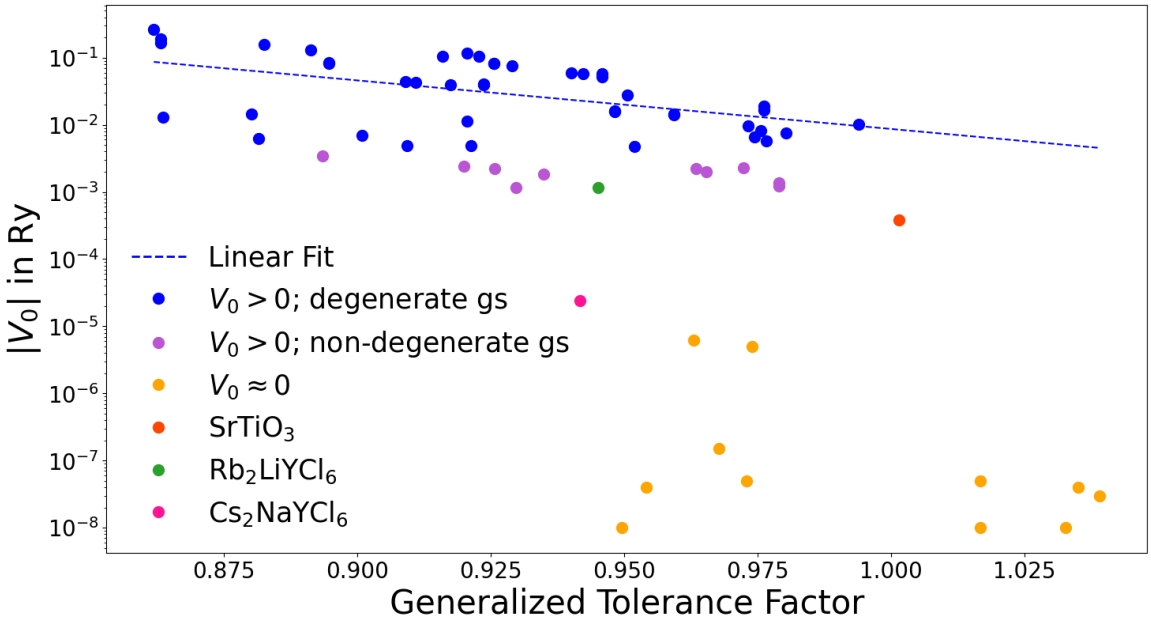

Figure 5.11: Absolute value of the potential height V_0 in semi-logarithmic representation as a function of the generalized tolerance factor t, as shown in fig. 5.10. However, a distinction was made here between the ferroelectrics with degenerate ground state (blue) and non-degenerate ground state (purple). The non-degenerate crystal structures are closer to the quantum paraelectric region.

(blue). It can be seen that the ferroelectric crystal structures with the non-degenerate ground state can be found below the linear fit. They are therefore closer to the quantum paraelectric region than the crystals with a degenerate ground state, which seems reasonable, since the quantum paraelectrics have a degenerate ground state, as seen in e.g. strontium titanate. These double perovskites would be interesting for an investigation of possible phase transitions from the ferroelectric to the paraelectric, but this is beyond the scope of this work.
Figure 5.12 shows the potential heights V_0 as a function of the average octahedral factor (upper image) and the octahedral mismatch (lower image). The two factors were calculated using equations (5.3) and (5.4). Both figures have a similar structure: the ferroelectric materials are distributed in the upper area. These are again divided into those that have a non-degenerate ground state (purple) and those that have a degenerate ground state (blue). The paraelectrics (orange) are found in the lower region with a tendency to have a smaller average octahedral factor or octahedral mismatch. This can be explained by the fact, that having a smaller octahedral factor indicates fewer distortions and thus a more stabilized structure. The non-degenerate ferroelectrics are found in the lower region of the group of ferroelectrics and thus again occupy a region closer to the quantum paraelectrics. As with the correlation plot of the tolerance factor, Cs_2NaYCl_6 (pink) lies in the area between the ferroelectrics and paraelectrics in both plots, while Rb_2LiYCl_6 (green) lies in the area of the ferroelectric materials in both cases. Strontium titanate is not be considered as a reference value here, as only one octahedral factor (see eq. (5.2)) is defined for single perovskite structures.

In figure 5.13 the same correlations are depicted in a different way. The three dimensional plots show the correlation of the tolerance factor t, the average octahedral factor $\bar{\mu}$ and the potential height V_0 (left image), as well as the correlation between the tolerance factor t and the octahedral mismatch $\Delta\mu$ and the potential height V_0 (right image). The different colors in the plots indicate the different potential heights. In order to be able to define a clear geometric shape, one would have to consider more double perovskites.
The two dimensional correlation plots show that there is a connection between the potential height and the tolerance factor, the average octahedral mismatch and the octahedral mismatch: areas can be defined in the correlation plots where double perovskites of the same phase can be found. With these results, a hypothesis could now be made as to which phase a double perovskite is in, based on only DFT calculations and the highly symmetric state, without solving the Schrödinger equation.

5.2.3 Centrosymmetric Structure

In all the structures calculated so far with Quantum ESPRESSO, a highly symmetric structure at zero displacement was used as a starting point for the calculations. In some cases, however, this resulted in very high potential barriers, which leads to the conclusion that the highly symmetric structure may not be the most energetically favorable one. If one imagines the double-well potential in three dimensions, for example in the form of a mexican hat potential, and cuts vertically through the potential landscape, then, depending on the cut, a different potential landscape could be the result. One approach for generating a structure that provides a lower potential surface could be the construction of a centrosymmetric structure. This structure would still have the necessary symmetry, but could allow octahedral tilting, which could lead to a lower energy barrier.
To generate this structure, the displaced, distorted structure in the minimum of the double well is inverted. This means that its now possible to display the other minimum of the double well potential through the inverted, equally distorted structure. A way to verify, if the structure is successfully inverted is to calculate its energy, since the double-well potential is symmetric and as a consequence the structures in the minima should have the same energy. Now the inverted and displaced structures are interpolated, resulting in a centrosymmetric structure at zero displacement that is similar to the highly symmetric one, but with slight differences in the coordinates. This can be seen in the example of Sr_2LaNbO_6 in graphic 5.14: on the left side, the highly symmetric, cubic structure can be seen in three-dimensional view (a) and along the a-axis (c). In comparison, the centrosymmetric structure can be seen on the right side in the three dimensional way (b) as well as from the view along the a-axis (d). From this comparison it can be seen, that the octahedra of the centrosymmetric structure are slightly tilted.
For the centrosymmetric structure, the energy can now be calculated using an SCF calculation, as well as the frequency of the system using a phonon calculation at the Γ point. The energy that the particle would have at the minimum of the double-well potential, which would result when doing the whole calculation (see procedure in figure 4.3) with the centrosymmetric structure as a starting point, is equal to the energy that the particle has at the minimum of the double-well, when starting the calculation

with the highly symmetric structure. The reason for that is, that since the potential can be described by an energy gradient, this state in the minimum is already the lowest in terms of energy. This was verified by recalculation. The centrosymmetric double well potential can therefore be calculated via the frequency and energy of the centrosymmetric structure and the energy of the displaced symmetric structure in the minimum. This is depicted in figure 5.15.
For the new centrosymmetric potential the Schrödinger equation can now be solved and the energy eigenvalues can be determined. The result of this calculation for Sr_2LaNbO_6 can be seen in figure 5.16. The blue dashed line represents the potential with the highly symmetric structure as the initial state at zero displacement. The potential height is calculated from the energy difference between the symmetric structure E_{sym} and the distorted, displaced structure E_{disp}, which results in 1160.161 meV. The corresponding solutions of the Schrödinger equation are shown in blue and orange for the degenerate ground state, which has a value of $E_0^{sym} = E_1^{sym} = 11.054\,\text{meV}$. The probability density is localized in the minima of the potential. The new centrosymmetric potential, which is calculated from the energy difference between the centrosymmetric structure E_{centro} and the distorted, displaced structure E_{disp}, is shown here in red. The potential height here is only 148.393 meV, so it has decreased by 1011.768 meV. The energy for the ground state, which is degenerate again, has also decreased. It is now $E_0^{centro} = E_1^{centro} = 5.239\,\text{meV}$. The eigenstates, shown in pink and green, are again localized in the minima. All four representations of the eigenstates have been enlarged in order to be able to recognize the different shapes.
It can therefore be stated that the construction of a centrosymmetric structure can lead to a reduction in the potential barrier, which is demonstrated using the example of Sr_2LaNbO_6. Despite the reduction of the energy barrier, Sr_2LaNbO_6 can still be classified as a ferroelectric. This raises the question of whether it is possible to use this symmetry consideration on other structures with a large potential energy barrier to find a structure that is more energetically favorable and would in turn reduce the potential barrier. This could perhaps lead to a quantum paraelectric state. However, this is beyond the scope of the present work, but could be an interesting starting point for future work.

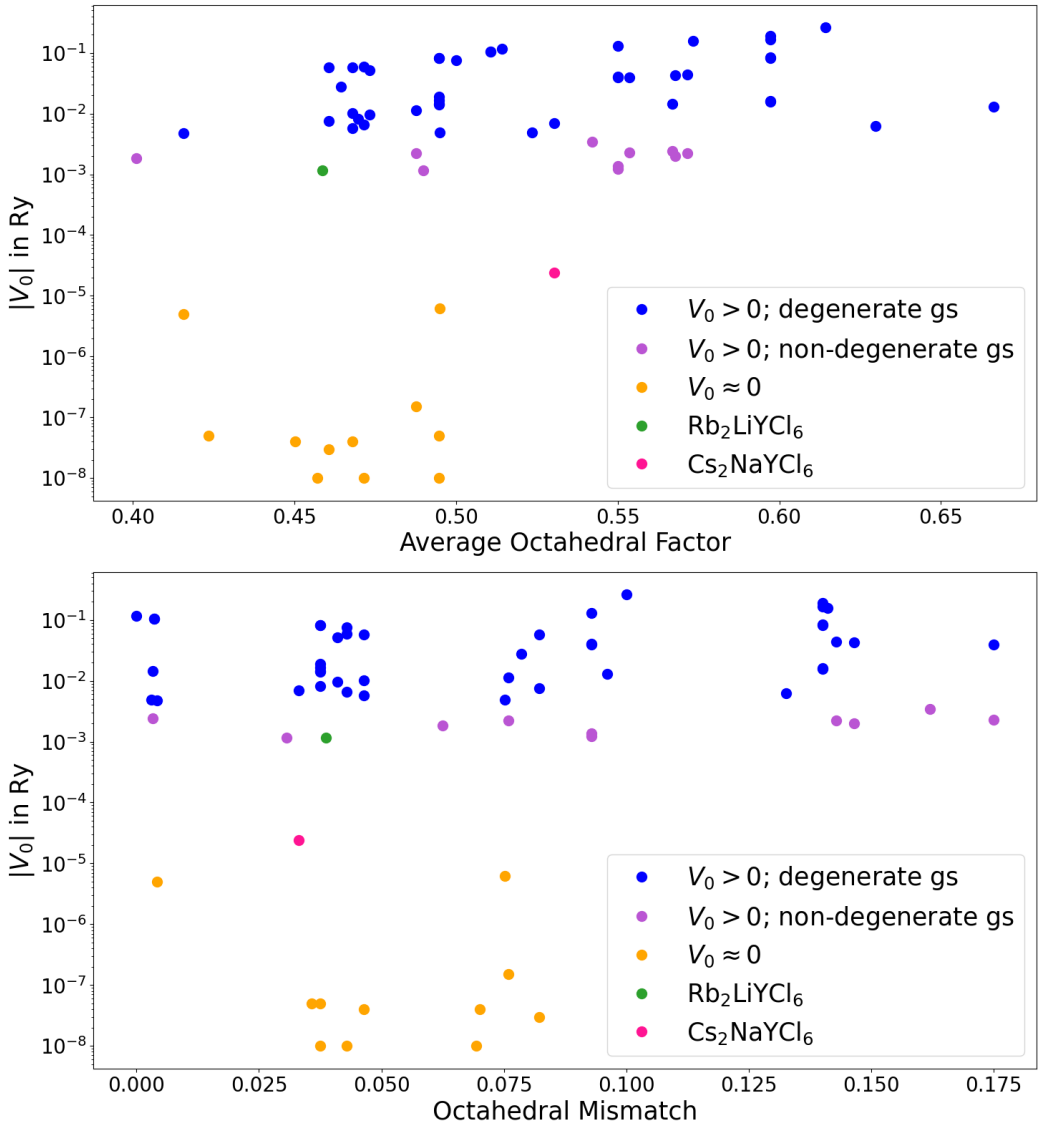

Figure 5.12: **Top**: Potential height V_0 as a function of the average octahedral factor $\bar{\mu}$.
Bottom: Potential height V_0 as a function of the octahedral mismatch $\Delta\mu$.
In both figures, the ferroelectrics with a degenerate ground state (gs) (in blue) and non-degenerate ground state (in purple) occupy the upper region of the plot, while the paraelectrics (orange) can be found in the lower left region. Again, the double perovskites with a degenerate ground state are located in the lower region of the ferroelectrics and thus closer to the quantum paraelectrics. Cs_2NaYCl_6 (pink) is again closer to the paraelectrics, while Rb_2LiYCl_6 (green) is in the ferroelectrics region.

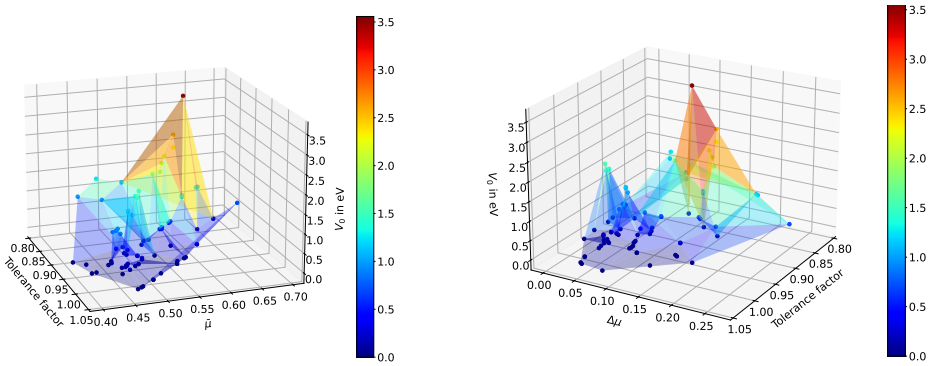

Figure 5.13: 3D representation of the correlation between the tolerance factor t, the average octahedral factor $\bar{\mu}$ and the potential height V_0 (left image), as well as the correlation between the tolerance factor t, the octahedral mismatch $\Delta\mu$ and the potential height V_0 (right image). The colors in the plot indicate the corresponding potential heights. With more double perovskites, investigated in the future, it should be possible to discern a defined geometric shape.

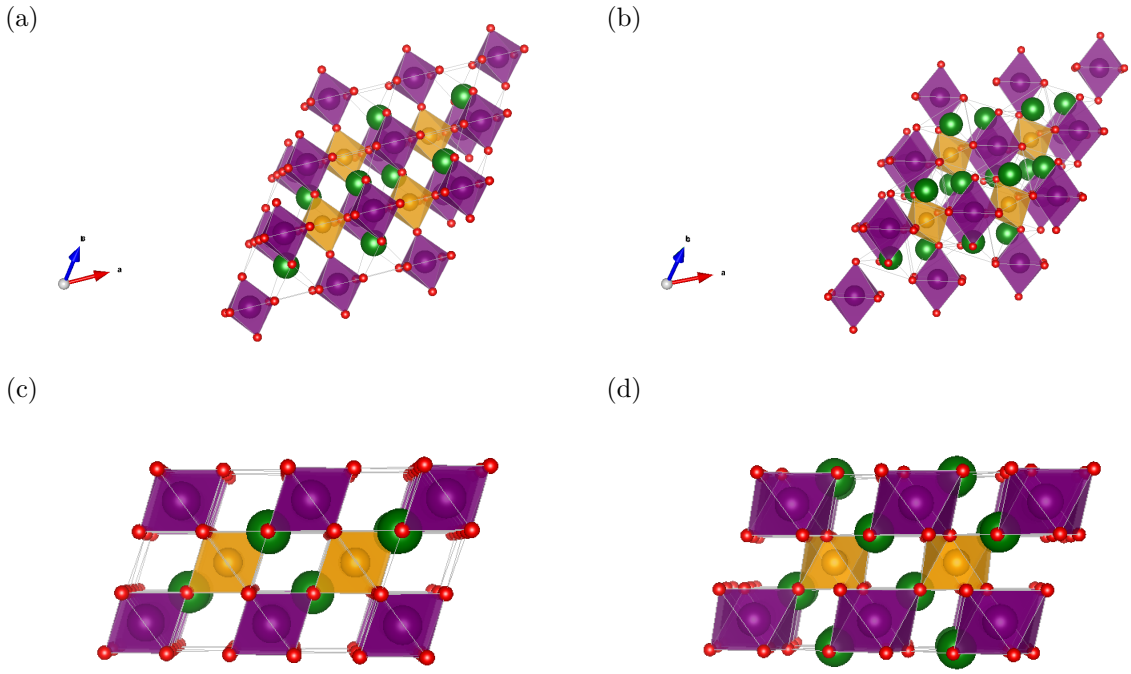

Figure 5.14: (**a**): Highly symmetric, cubic structure of Sr_2LaNbO_6. The strontium ions (green) are in between of the octahedrals from the lanthanum ions (purple) and the niobium ions (orange).
(**b**) Centrosymmetric structure of Sr_2LaNbO_6, where the tilting of the octahedra can be seen.
(**c**) Highly symmetric structure of Sr_2LaNbO_6 along the a-axis.
(**d**) Centrosymmetric structure of Sr_2LaNbO_6 along the a-axis. [4]

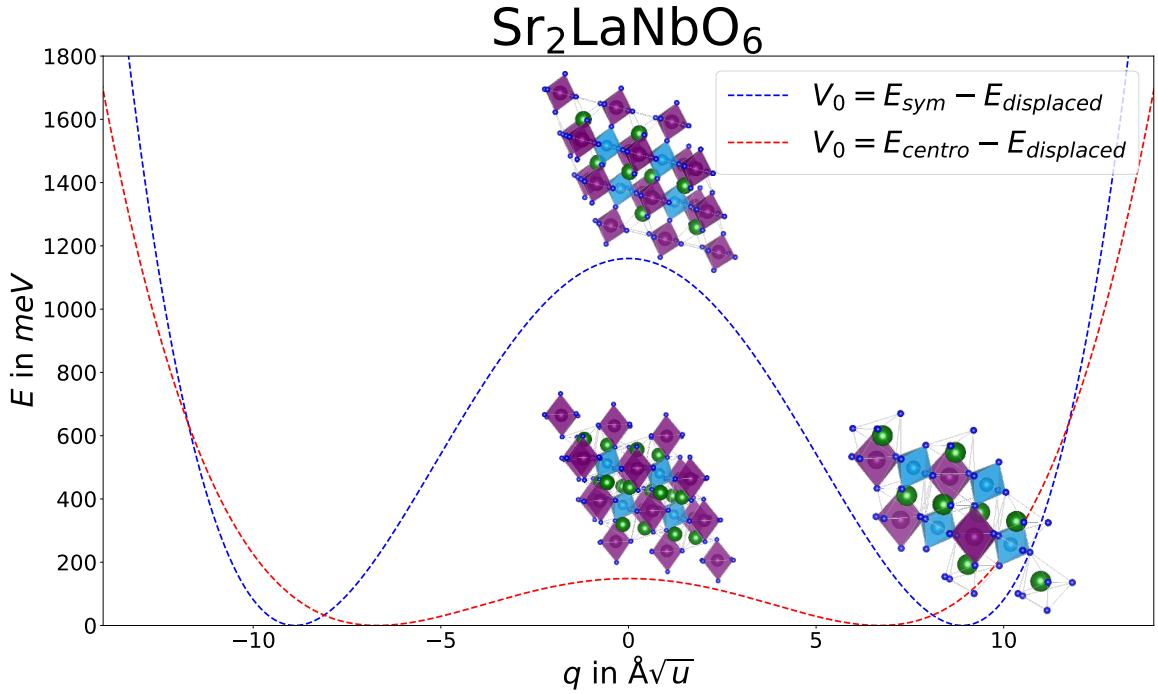

Figure 5.15: Potential of the highly symmetric structure (blue dashed line) with the potential barrier calculated through the energy difference of the symmetric structure (above the blue dashed line) and the distorted structure (in the minimum of the double well) as well as the potential of the centrosymmetric structure (red dashed line) for which the potential barrier can be extracted from the energy difference of the centrosymmetric structure (above the red line) and the distorted structure (in the minimum of the double well) for Sr_2LaNbO_6. It can be seen that the centrosymmetric structure is energetically more favorable due to the lower potential barrier.

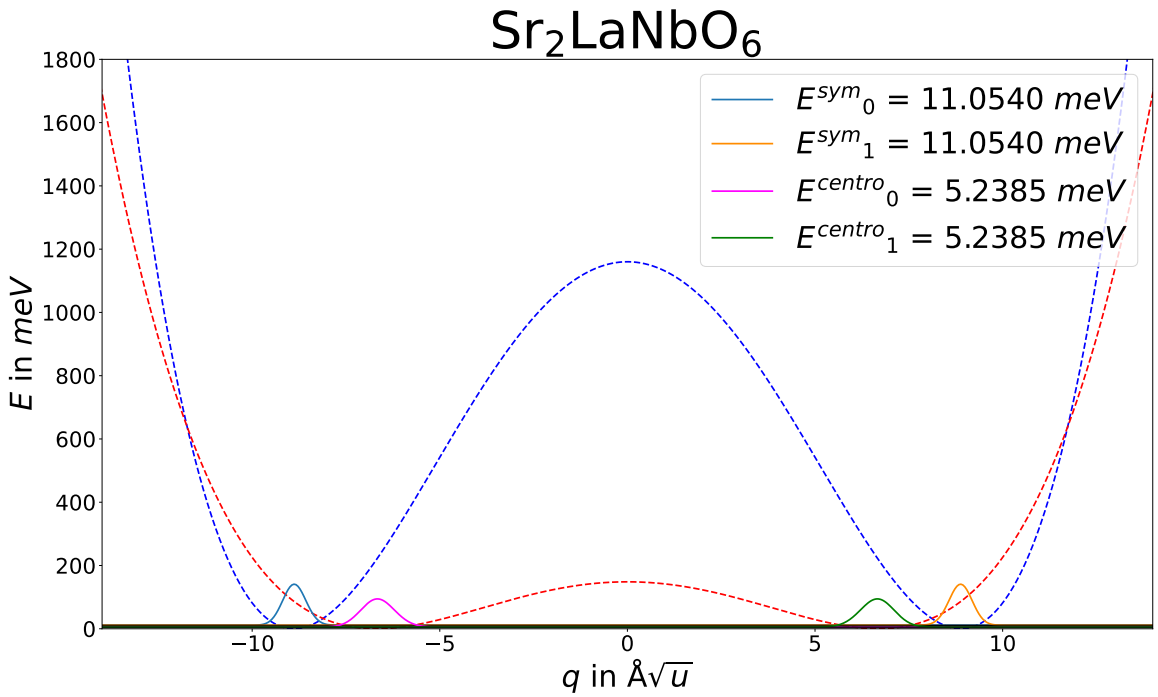

Figure 5.16: Potentials of the highly symmetric structure (blue dashed line) with the corresponding solutions (blue, orange) of the Schrödinger equation for the degenerate ground state, as well as the potential of the centrosymmetric structure (red dashed line) with their respective solutions (pink, green) for Sr_2LaNbO_6. It can be seen that the centrosymmetric structure is energetically more favorable due to the lower potential barrier. However in this case, the double perovskite remains in a ferroelectric phase, as its eigenstates are still localized in the minima of the potential.

Chapter 6

Conclusion and Outlook

This thesis investigates the question of whether quantum paraelectricity can be found in double perovskites.
First, quantum paraelectricity is investigated using the case study of strontium titanate, which has a simple perovskite structure. For this purpose, a method is utilized that made it possible to construct a double-well potential with the help of Quantum ESPRESSO calculations. The structure under consideration is imagined as a single particle for quantum mechanical consideration, which is localized at the maximum of a double-well potential. The calculation starts with a highly symmetric crystal structure at zero polarization. After a relaxation calculation, the energy of the initial structure can be determined through of a self-consistent field (SCF) calculation, and the frequency at the Γ point can be determined by a phonon calculation, which results in eigenvectors corresponding to negative frequencies due to the instability of the structure. The structure is afterwards shifted along those eigenvectors, which results in a removed position from the maximum. A further relaxation calculation leads the structure to be displaced into one of the minima of the double-well potential. The energy of the displaced structure can be calculated using an SCF calculation. The double-well potential used for solving a Schrödinger equation can be constructed through the potential barrier V_0 and the half width σ. The potential barrier can be obtained from the energy difference between the initial symmetric structure and the displaced structure at the end. The width from the maximum of the potential to a minimum, σ, can be calculated from V_0 and the frequency of the symmetric structure at the Γ point. With this double-well potential, the one-particle one-dimensional Schrödinger equation can be solved numerically and the energy eigenvalues obtained. This method is based on [1], who applied this method for several single perovskites, including strontium titanate.
For strontium titanate, a potential height of $V_0 = 5.22\,\mathrm{meV}$ and a value for σ of $0.623\,\text{Å}\sqrt{\mathrm{u}}$ are obtained. The solution of the Schrödinger equation results in a ground state energy of $6.24\,\mathrm{meV}$, which is close to the potential height. The fact that the probability density is delocalized over both minima leads to the conclusion that strontium titanate is a quantum paraelectric material. The calculated values deviate slightly from the reference calculation of [1], however, these values seem reasonable to make this method suitable to determine the phase of a perovskite. The deviation might origin from the use of slightly different parameters for the calculation.
The same method has been applied to a bulk of 77 double perovskites, which have

the same electronic configuration as strontium titanate. The result of this calculation show that, starting from a highly symmetric, cubic structure at zero displacement, 62 materials have a ferroelectric character, since their probability density is localized in one of the two minima of the double well potential and the ground state energy is well below the potential barrier. Of these 62 materials, 11 have a non-degenerate ground state, meaning a ground state that has a lower energy value than the first excited state. What is also noteworthy is that the potential barrier assumes values from approximately 30 meV to approximately 3500 meV.
13 of the 77 materials have a potential height of approximately 0 meV, which means that no double-well potential can be constructed. Instead the materials can be described using a parabola, which is why these materials can be classified as paraelectric. Two of the considered materials exhibit quantum paraelectric behavior: Cs_2NaYCl_6 and Rb_2LiYCl_6. For both, a double-well potential can be calculated and a probability density of the ground state delocalized over both minima can be found.
Using geometric factors that characterize the stability of perovskite structures, it is possible to find regions that separate the ferroelectrics from the paraelectrics as a function of the potential barrier. The quantum paraelectric materials are located in between the two regions. The ferroelectric double perovskites with a non-degenerate ground state tend to lie closer to the region of the quantum paraelectrics, who, according to calculations, have a non-degenerate ground state. These materials could be interesting subjects for future work. If the tolerance factor is considered as a function of the potential height, an exponential relationship can even be established in the area of the ferroelectric materials.
The large difference in the potential differences can indicate that the symmetric initial structure is not the most energetically favorable. In order to find a structure that can lower the potential height, a centrosymmetric structure is constructed that potentially allows tilting of the octahedra. Using Sr_2LaNbO_6 as an example, it can be shown that the potential barrier can indeed be lowered from 1160.161 meV to 148.393 meV. However, the solutions of the Schrödinger equation show that this structure remains in a ferroelectric state even with the centrosymmetric structure. This raises the question of whether double perovskites can be found in which the centrosymmetric structure leads to a quantum paraelectric state. This could be of interest for future work.
In summary, in this thesis it can be reproduced that strontium titanate is a quantum paraelectric material and after investigating different double perovskites, two materials are found, Cs_2NaYCl_6 and Rb_2LiYCl_6, that also exhibited quantum paraelectric behavior. In addition, it appears that a clear geometric origin of quantum paraelectricity exists. These results may provide valuable insights for future research for double perovskites, whose electronic configuration differs from those of strontium titanate.

Chapter 7

Danksagung

Zunächst bedanke ich mich bei Prof. Dr. Fabio Caruso für die sehr gute Betreuung, die inspirierenden Ideen und die wertvollen Ratschläge. Seine fachliche Kompetenz und geduldige Unterstützung haben diese Arbeit maßgeblich vorangebracht.

Desweiteren danke ich den Mitgliedern der Arbeitsgruppe, insbesondere Yiming Pan und Christoph Emeis, für hilfreichen Diskussionen und die Bereitschaft, mir bei Fragen und Problemen jederzeit zur Seite zu stehen.

Nicht zuletzt danke ich meiner Familie und meinen Freunden für ihre konstante Unterstützung und ihre motivierenden Worte.

Appendix A

Convergence Tests and Tables

A.1 Convergence Tests for $SrTiO_3$

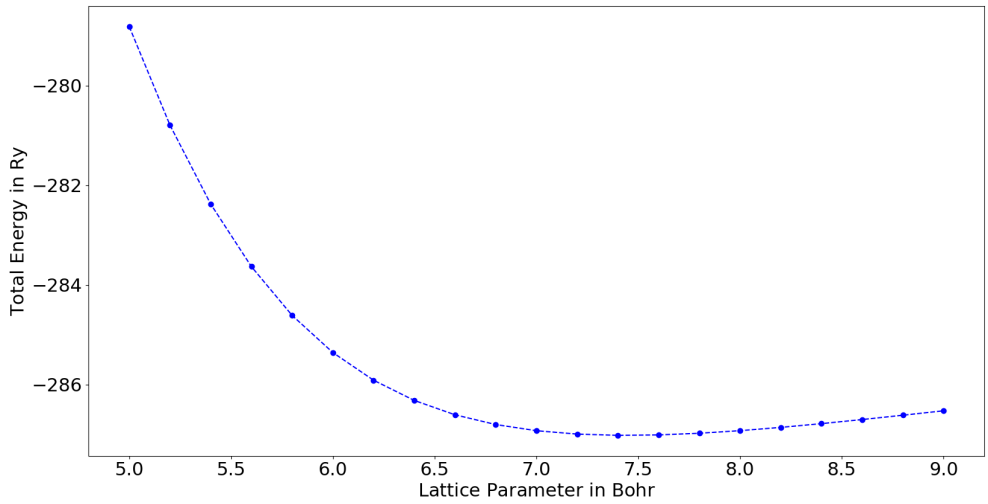

Figure A.1: Convergence test for the lattice constant of $SrTiO_3$. A lattice parameter of $7.4\,a_0$ was selected for the calculation.

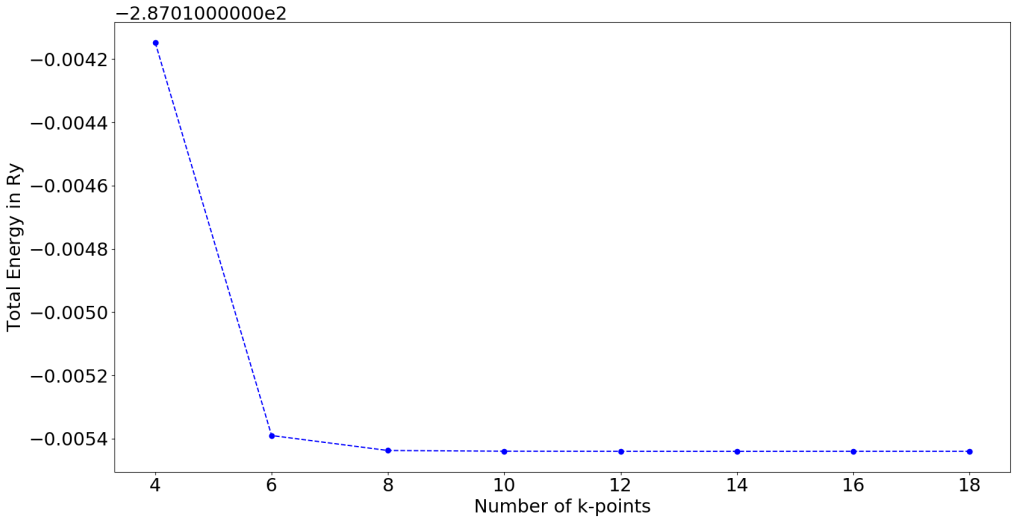

Figure A.2: Convergence test for the k-point grid for $SrTiO_3$. For the calculations a $8 \times 8 \times 8$ grid was chosen.

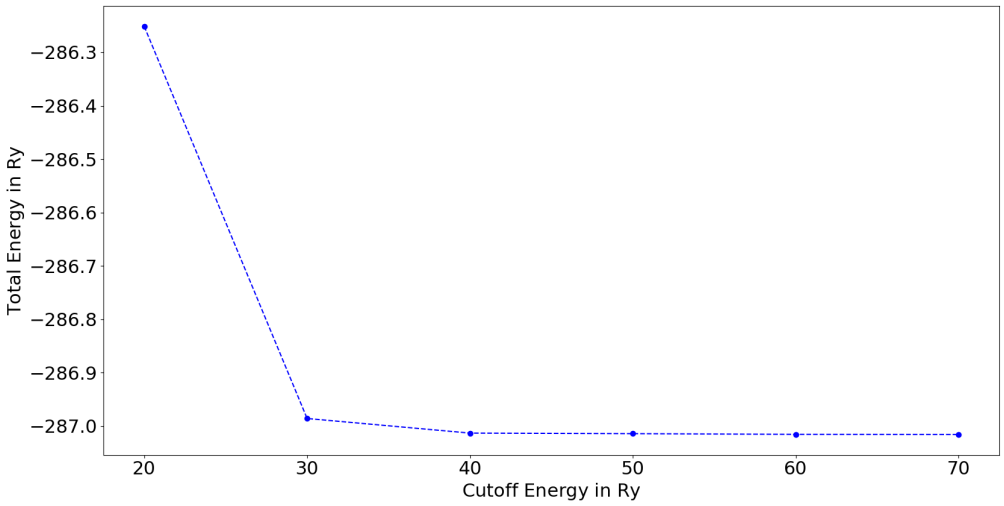

Figure A.3: Convergence test the cut-off energy of $SrTiO_3$. For the calculations a cut-off energy of 60 Ry was used.

A.2 Convergence Tests for Sr_2CaWO_6

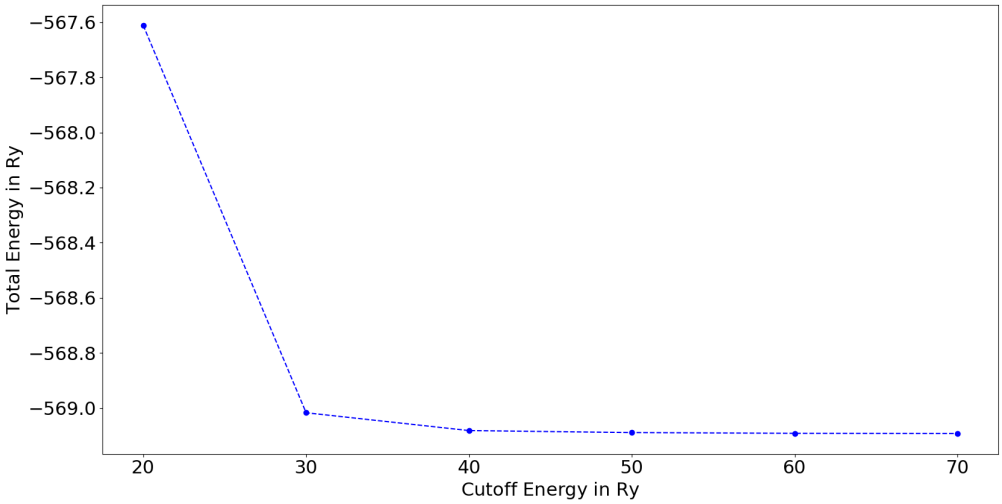

Figure A.4: Convergence test for the cutoff-Energy of Sr_2CaWO_6. The calculations of the double Perovskites were carried out with 60 Ry.

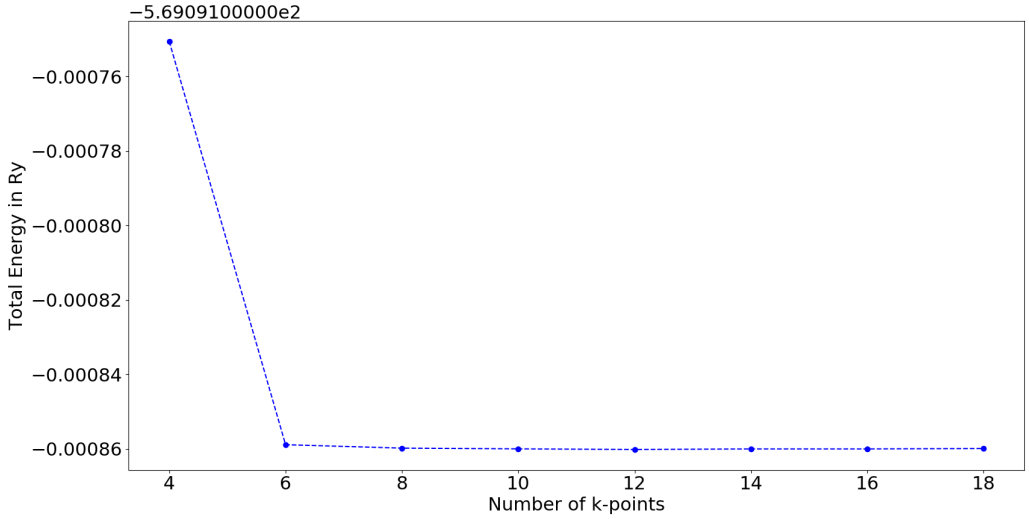

Figure A.5: Convergence test for the k-point grid of Sr_2CaWO_6. An $8 \times 8 \times 8$ grid was selected for the calculations of the double perovskites.

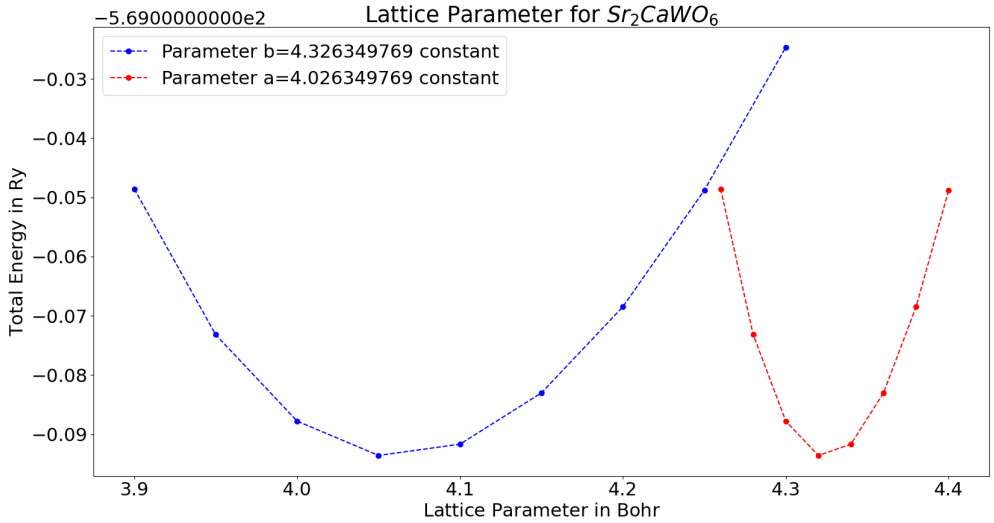

Figure A.6: Convergence test for the lattice parameter of Sr_2CaWO_6. In Quantum ESPRESSO it is possible to set the lattice parameter via one constant or through a 3×3 matrix, which was used here. The matrix for the lattice parameters is of the form $[(a, 0, b), (a, a, 0), (0, a, b)]$. In the convergence tests, one of these parameters was fixed while the other was changed. This results in a value of a of $4.026\,349\,769\,a_0$ and a value of b of $4.326\,349\,769\,a_0$. Combining the two values, the lattice constant resulted in $11.17\,a_0$.

A.3 Results of the Schrödinger Equation for Double Perovskites

Element	E_{sym} in Ry	E_{dipl} in Ry	ω in THz	V_0 in Ry	V_0 in eV	σ in Å$\sqrt{\text{u}}$	M_l in u
Sr_3MoO_6	-544.5407	-544.625	-5.9456	0.0843	1.1466	8.8457	15.999
Sr_2NaReO_6	-620.8728	-620.9121	-5.3258	0.0393	0.5349	6.7444	15.999
Sr_2ScNbO_6	-547.7637	-547.7781	-4.6868	0.0144	0.196	4.6389	15.999
Sr_2TiZrO_6	-553.972	-553.9816	-4.3341	0.0096	0.1305	4.0937	15.999
Sr_2ScTaO_6	-571.7655	-571.7794	-4.6788	0.0139	0.1895	4.5691	15.999
Sr_2YNbO_6	-546.2069	-546.2471	-5.638	0.0402	0.5467	6.4414	15.999
Sr_2LaTaO_6	-579.8533	-579.9349	-5.9157	0.0815	1.1089	8.7429	15.999
Sr_2MgMoO_6	-599.8228	-599.8286	-3.8795	0.0058	0.0787	3.5526	15.999
Sr_3WO_6	-564.4216	-564.5061	-5.9415	0.0845	1.1488	8.86	15.999
Sr_2LiReO_6	-540.08	-540.0876	-3.9946	0.0076	0.1029	5.9871	6.941
Sr_2CaWO_6	-569.2948	-569.3386	-5.6405	0.0439	0.5967	6.7264	15.999
Sr_2YTaO_6	-570.2112	-570.2505	-5.6136	0.0393	0.5349	6.3992	15.999
Sr_2LaNbO_6	-555.8487	-555.934	-5.9505	0.0853	1.1602	8.8904	15.999
Sr_2CaMoO_6	-549.4156	-549.4581	-5.6259	0.0425	0.578	6.6371	15.999
Sr_2TiHfO_6	-613.627	-613.6351	-4.2017	0.0081	0.1106	3.8872	15.999
Sr_2MgWO_6	-619.6985	-619.705	-3.8579	0.0065	0.0888	3.794	15.999
Rb_2LiYCl_6	-414.9066	-414.9077	-10.0801	0.0012	0.0159	0.9316	6.941
La_2MgTiO_6	-644.9725	-645.0247	-7.0366	0.0522	0.7096	5.8798	15.999
Pb_2MgMoO_6	-787.2222	-787.2323	-4.4602	0.0101	0.1373	4.0805	15.999
Ba_2ScTaO_6	-572.0352	-572.0352	-1.3341	-0.0	-0.0	NaN	15.999
Ba_2MgMoO_6	-600.0812	-600.0812	-0.6425	-0.0	-0.0	NaN	15.999
Ca_2LaNbO_6	-565.2894	-565.4781	-7.4855	0.1887	2.5669	10.5123	15.999
$Rb_2LiScCl_6$	-416.3655	-416.3655	-3.8828	-0.0	-0.0	NaN	6.941
Ba_3WO_6	-564.7964	-564.8482	-4.9861	0.0517	0.7035	8.262	15.999
Cs_2NaScI_6	-710.7331	-710.735	-4.5624	0.0019	0.0254	1.4314	22.99
Cs_2LiYBr_6	-515.8612	-515.8612	-11.9851	0.0	0.0	0.0051	6.941
Pb_2ScTaO_6	-759.1743	-759.1908	-4.7691	0.0165	0.2244	4.8781	15.999
$Cs_2NaLaCl_6$	-525.3856	-525.388	-2.9811	0.0024	0.0331	2.499	22.99
Ca_3MoO_6	-558.8734	-559.0003	-7.2894	0.1269	1.7253	8.8503	15.999
Ba_2CaMoO_6	-549.7291	-549.731	-2.8263	0.002	0.0271	2.8585	15.999
Ca_3WO_6	-578.752	-578.8945	-7.2821	0.1425	1.9377	9.3886	15.999
Na_3YCl_6	-579.985	-580.0664	-2.6993	0.0814	1.1076	15.9742	22.99
Ba_2CaWO_6	-569.6078	-569.61	-2.8202	0.0022	0.0301	3.0204	15.999
$Cs_2NaScBr_6$	-598.1957	-598.1957	-3.0417	-0.0	-0.0	NaN	22.99
$Rb_2NaScCl_6$	-497.2408	-497.243	-4.0145	0.0022	0.0299	1.7651	22.99
Ca_2ScTaO_6	-581.2487	-581.3298	-6.8975	0.0811	1.1025	7.4766	15.999
Ca_2YTaO_6	-579.6716	-579.8024	-7.2334	0.1308	1.779	9.0566	15.999
Cs_2NaYCl_6	-515.631	-515.631	-3.3188	2.4e-05	0.0003	0.2248	22.99
$Cs_2NaLaBr_6$	-606.5097	-606.5145	-2.6578	0.0049	0.0662	3.9655	22.99
Ba_2NaReO_6	-621.1871	-621.1894	-2.9425	0.0023	0.0308	2.9314	15.999
$Cs_2LiLaBr_6$	-525.6306	-525.6306	-12.6873	0.0	0.0	0.0022	6.941

Continued on next page

Element	E_{sym} in Ry	E_{dipl} in Ry	ω in THz	V_0 in Ry	V_0 in eV	σ in Å$\sqrt{\text{u}}$	M_l in u in u
Ba_2LaNbO_6	-556.1866	-556.2027	-4.1615	0.0161	0.2188	5.521	15.999
$Rb_2NaLaCl_6$	-505.5298	-505.5442	-2.8514	0.0144	0.1958	6.359	22.99
Ba_2ScNbO_6	-548.0348	-548.0348	-1.6308	-0.0	-0.0	NaN	15.999
La_2LiVO_6	-559.7251	-559.7526	-6.2142	0.0275	0.3741	7.3391	6.941
Cs_2KScBr_6	-559.8601	-559.8635	-4.2344	0.0035	0.047	1.6086	39.098
$K_2LiScCl_6$	-424.0161	-424.0208	-3.8408	0.0048	0.0646	4.9358	6.941
La_2LiNbO_6	-532.6182	-532.6942	-7.4342	0.076	1.0332	10.1954	6.941
Ca_2LiReO_6	-549.5751	-549.6324	-6.5578	0.0573	0.7791	10.0369	6.941
Cs_2LiYCl_6	-434.749	-434.749	-10.7862	0.0	0.0	0.0	6.941
Cs_2KYCl_6	-477.2894	-477.2956	-3.7147	0.0062	0.0838	2.5719	35.453
Rb_2NaYCl_6	-495.7801	-495.787	-3.1077	0.007	0.095	4.0629	22.99
Ba_2MgWO_6	-619.9563	-619.9563	-0.2188	-0.0	-0.0	NaN	15.999
La_2CaTiO_6	-594.4772	-594.6353	-8.3242	0.1581	2.1497	8.6509	15.999
Pb_2ScNbO_6	-735.173	-735.192	-4.8218	0.0191	0.2595	5.1893	15.999
Ca_2MgWO_6	-629.1947	-629.2539	-6.6217	0.0592	0.8055	6.6572	15.999
$Cs_2NaScCl_6$	-517.0862	-517.0862	-4.3579	-0.0	-0.0	NaN	22.99
Ba_2LiReO_6	-540.3542	-540.3542	-0.5148	-0.0	-0.0	NaN	6.941
Na_3YBr_6	-661.0869	-661.1782	-2.4717	0.0914	1.2424	18.4765	22.99
$Cs_2LiLaCl_6$	-444.5069	-444.5069	-11.4075	-0.0	-0.0	NaN	6.941
Na_3ScCl_6	-581.455	-581.518	-3.217	0.0631	0.8578	11.7957	22.99
Ba_2YVO_6	-573.516	-573.516	-1.6796	0.0	0.0	0.0	15.999
$Tl_2NaScCl_6$	-680.5579	-680.5693	-4.5042	0.0114	0.1548	3.5791	22.99
Cs_2KLaCl_6	-487.0418	-487.0548	-3.2951	0.0131	0.1778	4.2223	35.453
Ca_2MgMoO_6	-609.3198	-609.3769	-6.5967	0.0571	0.7768	6.5621	15.999
Ba_2LaTaO_6	-580.1904	-580.2059	-4.0842	0.0155	0.2108	5.5218	15.999
Ca_2ZrHfO_6	-603.0427	-603.1476	-7.0896	0.1048	1.4254	8.271	15.999
Ca_2LaTaO_6	-589.2942	-589.4581	-7.4586	0.1639	2.2285	9.8303	15.999
Ba_2YNbO_6	-546.514	-546.5154	-2.6186	0.0014	0.0188	2.5743	15.999
$Rb_2LiLaCl_6$	-424.6581	-424.663	-10.7522	0.0049	0.0662	1.7842	6.941
Cs_2NaYBr_6	-596.7437	-596.7448	-2.9516	0.0011	0.0156	1.7344	22.99
Ca_2ScNbO_6	-557.2465	-557.3296	-6.9056	0.083	1.129	7.5573	15.999
Ba_2YTaO_6	-570.5171	-570.5183	-2.5102	0.0012	0.0165	2.516	15.999
La_2CaZrO_6	-574.343	-574.6046	-8.8527	0.2616	3.5575	10.4644	15.999
La_2MgHfO_6	-684.5031	-684.6082	-7.8721	0.105	1.4282	7.4561	15.999
Na_3ScBr_6	-662.5504	-662.6213	-2.849	0.0709	0.9648	14.126	22.99

Continued on next page

Element	E_{sym} in Ry	E_{dipl} in Ry	ω in THz	V_0 in Ry	V_0 in eV	σ in Å$\sqrt{\text{u}}$	M_l in u in u
La_2MgZrO_6	-624.8413	-624.9575	-7.9463	0.1163	1.5815	7.7729	15.999

Table A.1: Energy values of the highly symmetrical structure E_{sym} at zero displacement, the polar, shifted structure E_{displ}, as well as the frequencies ω of the highly symmetrical structure at the Γ point. In addition, the potential barrier V_0 was calculated via $V_0 = E_{sym} - E_{displ}$ in Ry and converted into eV. The half-width of the potential σ was calculated using eq. (3.4). M_l indicates the mass of the lightest ion of the compound, here given by Oxygen ($M_l = 15.999u$), Lithium ($M_l = 6.941u$), Sodium ($M_l = 22.99u$), Potassium ($M_l = 39.098u$) or Chlorine ($M_l = 35.453u$) [30]. This was used to convert the σ value into units of Å$\sqrt{\text{u}}$.
Some of the potential barriers are negative or zero. These elements can be assumed to be paraelectrics, as a parabolic image must be used here to explain the values and the image of a double well can't be applied here. The paraelectric elements are [$Cs_2LiLaBr_6$, Cs_2LiYBr_6, Ba_2ScTaO_6, Ba_2MgMoO_6, $Rb_2LiScCl_6$, $Cs_2NaScBr_6$, Ba_2ScNbO_6, Cs_2LiYCl_6, Ba_2MgWO_6, $Cs_2NaScCl_6$, Ba_2LiReO_6, $Cs_2LiLaCl_6$, Ba_2YVO_6] For those elements the value of V_0 in Ry is zero, because either the potential height had a value of zero, the potential height had a very small negative value (due to numerical inaccuracies, which also lead to the NaN- values for σ in this cases) (e.g. $Cs_2NaScCl_6$, whose potential height was calculated to -1.5×10^{-7} Ry) or the potential height was so small, that no double well could be constructed and the potential height was set to zero (e.g. $Cs_2LiLaBr_6$, whose potential height was calculated to 1×10^{-8} Ry).

Element	V_0 in meV	E_1 in meV	E_2 in meV
Sr_3MoO_6	1146.63572	11.04485	11.04485
Sr_2NaReO_6	534.85427	9.88692	9.88692
Sr_2ScNbO_6	195.95424	8.67417	8.67417
Sr_2TiZrO_6	130.49744	8.00394	8.00394
Sr_2ScTaO_6	189.45589	8.65793	8.65793
Sr_2YNbO_6	546.73537	10.46573	10.46573
Sr_2LaTaO_6	1108.90986	10.98933	10.98933
Sr_2MgMoO_6	78.74373	7.13653	7.13653
Sr_3WO_6	1148.76752	11.03734	11.03734
Sr_2LiReO_6	102.87026	4.86777	4.86777
Sr_2CaWO_6	596.72135	10.47198	10.47198
Sr_2YTaO_6	534.93533	10.42003	10.42003
Sr_2LaNbO_6	1160.16146	11.054	11.054
Sr_2CaMoO_6	577.97076	10.44435	10.44435
Sr_2TiHfO_6	110.58582	7.75049	7.75049
Sr_2MgWO_6	88.81371	7.10697	7.10697
Rb_2LiYCl_6	15.85801	9.62336	12.21438
La_2MgTiO_6	709.60761	13.06284	13.06284
Pb_2MgMoO_6	137.3139	8.2383	8.2383
Ca_2LaNbO_6	2566.89718	13.90273	13.90273
Ba_3WO_6	703.4974	9.26063	9.26063
Cs_2NaScI_6	25.40412	9.51286	9.66827
Pb_2ScTaO_6	224.36124	8.83201	8.83201
$Cs_2NaLaCl_6$	33.0582	6.47396	6.47418
Ca_3MoO_6	1725.31273	13.54135	13.54135
Ba_2CaMoO_6	27.05856	5.12546	5.12557
Ca_3WO_6	1937.73045	13.52743	13.52743
Na_3YCl_6	1107.56958	6.00982	6.00982
Ba_2CaWO_6	30.07953	5.12906	5.12908
$Rb_2NaScCl_6$	29.90939	8.57862	8.59629
Ca_2ScTaO_6	1102.47244	12.81214	12.81214
Ca_2YTaO_6	1779.03844	13.43718	13.43718
Cs_2NaYCl_6	0.3317	7.85936	28.71312
$Cs_2NaLaBr_6$	66.17257	5.8625	5.8625
Ba_2NaReO_6	30.84385	5.34915	5.34918
Ba_2LaNbO_6	218.8376	7.71075	7.71075
$Rb_2NaLaCl_6$	195.84857	6.33548	6.33548
La_2LiVO_6	374.07262	7.59694	7.59694
Cs_2KScBr_6	47.00187	11.87893	11.88637
$K_2LiScCl_6$	64.63264	4.66516	4.66516
La_2LiNbO_6	1033.18547	9.09647	9.09647
Ca_2LiReO_6	779.13883	8.02379	8.02379

Continued on next page

Element	V_0 in meV	E_1 in meV	E_2 in meV
Cs_2KYCl_6	83.84822	10.12985	10.12985
Rb_2NaYCl_6	94.96132	6.8696	6.8696
La_2CaTiO_6	2149.67856	15.46331	15.46331
Pb_2ScNbO_6	259.53886	8.93502	8.93502
Ca_2MgWO_6	805.54745	12.29636	12.29636
Na_3YBr_6	1242.39577	5.50171	5.50171
Na_3ScCl_6	857.78355	7.16395	7.16395
$Tl_2NaScCl_6$	154.81383	9.96717	9.96717
Cs_2KLaCl_6	177.81184	9.07043	9.07043
Ca_2MgMoO_6	776.78358	12.24929	12.24929
Ba_2LaTaO_6	210.84474	7.56691	7.56691
Ca_2ZrHfO_6	1425.35929	13.17017	13.17017
Ca_2LaTaO_6	2228.50498	13.85431	13.85431
Ba_2YNbO_6	18.83818	4.70191	4.70451
$Rb_2LiLaCl_6$	66.18685	12.83413	12.83451
Cs_2NaYBr_6	15.6109	6.11275	6.24771
Ca_2ScNbO_6	1129.04861	12.82732	12.82732
Ba_2YTaO_6	16.53556	4.48884	4.49445
La_2CaZrO_6	3557.53737	16.4389	16.4389
La_2MgHfO_6	1428.17299	14.62338	14.62338
Na_3ScBr_6	964.81637	6.34399	6.34399
La_2MgZrO_6	1581.46512	14.76157	14.76157

Table A.2: Potential barrier V_0 for the respective elements, as well as the ground state energy E_0 and that of the first excited state E_1 for all materials that have a potential barrier greater than zero. It is noticeable that the ground state is non-degenerate for 13 of the 64 elements.

A.4 Ionic Radii and Geometric Factors

Element	A	B	B'	X	r_A in Å	r_B in Å	$r_{B'}$ in Å	r_X in Å	$\bar{\mu}$	$\Delta\mu$	t
Ba_2CaMoO_6	Ba	Ca	Mo	O	1.61	1.0	0.59	1.4	0.56786	0.14643	0.96545
Ba_2CaWO_6	Ba	Ca	W	O	1.61	1.0	0.6	1.4	0.57143	0.14286	0.96348
Ba_2LaNbO_6	Ba	La	Nb	O	1.61	1.032	0.64	1.4	0.59714	0.14	0.94824
Ba_2LaTaO_6	Ba	La	Ta	O	1.61	1.032	0.64	1.4	0.59714	0.14	0.94824
Ba_2LiReO_6	Ba	Li	Re	O	1.61	0.76	0.53	1.4	0.46071	0.08214	1.03914
Ba_2MgMoO_6	Ba	Mg	Mo	O	1.61	0.72	0.59	1.4	0.46786	0.04643	1.0352
Ba_2MgWO_6	Ba	Mg	W	O	1.61	0.72	0.6	1.4	0.47143	0.04286	1.03276
Ba_2NaReO_6	Ba	Na	Re	O	1.61	1.02	0.53	1.4	0.55357	0.175	0.97242
Ba_2ScNbO_6	Ba	Sc	Nb	O	1.61	0.745	0.64	1.4	0.49464	0.0375	1.01683
Ba_2ScTaO_6	Ba	Sc	Ta	O	1.61	0.745	0.64	1.4	0.49464	0.0375	1.01683
Ba_2YNbO_6	Ba	Y	Nb	O	1.61	0.9	0.64	1.4	0.55	0.09286	0.97907
Ba_2YTaO_6	Ba	Y	Ta	O	1.61	0.9	0.64	1.4	0.55	0.09286	0.97907
Ba_2YVO_6	Ba	Y	V	O	1.61	0.9	0.54	1.4	0.51429	0.12857	1.00036
Ba_3WO_6	Ba	Ba	W	O	1.61	1.35	0.6	1.4	0.69643	0.26786	0.8852
Ca_2LaNbO_6	Ca	La	Nb	O	1.34	1.032	0.64	1.4	0.59714	0.14	0.86318
Ca_2LaTaO_6	Ca	La	Ta	O	1.34	1.032	0.64	1.4	0.59714	0.14	0.86318
Ca_2LiReO_6	Ca	Li	Re	O	1.34	0.76	0.53	1.4	0.46071	0.08214	0.94592
Ca_2MgMoO_6	Ca	Mg	Mo	O	1.34	0.72	0.59	1.4	0.46786	0.04643	0.94234
Ca_2MgWO_6	Ca	Mg	W	O	1.34	0.72	0.6	1.4	0.47143	0.04286	0.94012
Ca_2ScNbO_6	Ca	Sc	Nb	O	1.34	0.745	0.64	1.4	0.49464	0.0375	0.92562
Ca_2ScTaO_6	Ca	Sc	Ta	O	1.34	0.745	0.64	1.4	0.49464	0.0375	0.92562
Ca_2YTaO_6	Ca	Y	Ta	O	1.34	0.9	0.64	1.4	0.55	0.09286	0.89125
Ca_2ZrHfO_6	Ca	Zr	Hf	O	1.34	0.72	0.71	1.4	0.51071	0.00357	0.91606
Ca_3MoO_6	Ca	Ca	Mo	O	1.34	1.0	0.59	1.4	0.56786	0.14643	0.87885
Ca_3WO_6	Ca	Ca	W	O	1.34	1.0	0.6	1.4	0.57143	0.14286	0.87705
Cs_2KLaCl_6	Cs	K	La	Cl	1.88	1.38	1.032	1.81	0.6663	0.09613	0.86369
Cs_2KScBr_6	Cs	K	Sc	Br	1.88	1.38	0.745	1.96	0.54209	0.16199	0.89344
Cs_2KYCl_6	Cs	K	Y	Cl	1.88	1.38	0.9	1.81	0.62983	0.1326	0.88157
$Cs_2LiLaBr_6$	Cs	Li	La	Br	1.88	0.76	1.032	1.96	0.45714	0.06939	0.94966
$Cs_2LiLaCl_6$	Cs	Li	La	Cl	1.88	0.76	1.032	1.81	0.49503	0.07514	0.96302
Cs_2LiYBr_6	Cs	Li	Y	Br	1.88	0.76	0.9	1.96	0.42347	0.03571	0.97292
Cs_2LiYCl_6	Cs	Li	Y	Cl	1.88	0.76	0.9	1.81	0.45856	0.03867	0.988
$Cs_2NaLaBr_6$	Cs	Na	La	Br	1.88	1.02	1.032	1.96	0.52347	0.00306	0.90934
$Cs_2NaLaCl_6$	Cs	Na	La	Cl	1.88	1.02	1.032	1.81	0.56685	0.00331	0.92003
$Cs_2NaScBr_6$	Cs	Na	Sc	Br	1.88	1.02	0.745	1.96	0.45026	0.07015	0.95413
$Cs_2NaScCl_6$	Cs	Na	Sc	Cl	1.88	1.02	0.745	1.81	0.48757	0.07597	0.96781
Cs_2NaScI_6	Cs	Na	Sc	I	1.88	1.02	0.745	2.2	0.40114	0.0625	0.935
Cs_2NaYBr_6	Cs	Na	Y	Br	1.88	1.02	0.9	1.96	0.4898	0.03061	0.9297
Cs_2NaYCl_6	Cs	Na	Y	Cl	1.88	1.02	0.9	1.81	0.53039	0.03315	0.94174
$K_2LiScCl_6$	K	Li	Sc	Cl	1.64	0.76	0.745	1.81	0.41575	0.00414	0.952
La_2CaTiO_6	La	Ca	Ti	O	1.36	1.0	0.605	1.4	0.57321	0.14107	0.88255
La_2CaZrO_6	La	Ca	Zr	O	1.36	1.0	0.72	1.4	0.61429	0.1	0.86189
La_2LiNbO_6	La	Li	Nb	O	1.36	0.76	0.64	1.4	0.5	0.04286	0.92896

Continued on next page

Element	A	B	B'	X	r_A in Å	r_B in Å	$r_{B'}$ in Å	r_X in Å	$\bar{\mu}$	$\Delta\mu$	t
La_2LiVO_6	La	Li	V	O	1.36	0.76	0.54	1.4	0.46429	0.07857	0.95064
La_2MgHfO_6	La	Mg	Hf	O	1.36	0.72	0.71	1.4	0.51071	0.00357	0.92275
La_2MgTiO_6	La	Mg	Ti	O	1.36	0.72	0.605	1.4	0.47321	0.04107	0.94587
La_2MgZrO_6	La	Mg	Zr	O	1.36	0.72	0.72	1.4	0.51429	0.0	0.92057
Na_3ScBr_6	Na	Na	Sc	Br	1.39	1.02	0.745	1.96	0.45026	0.07015	0.83238
Na_3ScCl_6	Na	Na	Sc	Cl	1.39	1.02	0.745	1.81	0.48757	0.07597	0.83929
Na_3YBr_6	Na	Na	Y	Br	1.39	1.02	0.9	1.96	0.4898	0.03061	0.81106
Na_3YCl_6	Na	Na	Y	Cl	1.39	1.02	0.9	1.81	0.53039	0.03315	0.81668
Pb_2MgMoO_6	Pb	Mg	Mo	O	1.49	0.72	0.59	1.4	0.46786	0.04643	0.99393
Pb_2ScNbO_6	Pb	Sc	Nb	O	1.49	0.745	0.64	1.4	0.49464	0.0375	0.97629
Pb_2ScTaO_6	Pb	Sc	Ta	O	1.49	0.745	0.64	1.4	0.49464	0.0375	0.97629
$Rb_2LiLaCl_6$	Rb	Li	La	Cl	1.72	0.76	1.032	1.81	0.49503	0.07514	0.92126
$Rb_2LiScCl_6$	Rb	Li	Sc	Cl	1.72	0.76	0.745	1.81	0.41575	0.00414	0.97408
Rb_2LiYCl_6	Rb	Li	Y	Cl	1.72	0.76	0.9	1.81	0.45856	0.03867	0.94516
$Rb_2NaLaCl_6$	Rb	Na	La	Cl	1.72	1.02	1.032	1.81	0.56685	0.00331	0.88014
$Rb_2NaScCl_6$	Rb	Na	Sc	Cl	1.72	1.02	0.745	1.81	0.48757	0.07597	0.92585
Rb_2NaYCl_6	Rb	Na	Y	Cl	1.72	1.02	0.9	1.81	0.53039	0.03315	0.9009
Sr_2CaMoO_6	Sr	Ca	Mo	O	1.44	1.0	0.59	1.4	0.56786	0.14643	0.91093
Sr_2CaWO_6	Sr	Ca	W	O	1.44	1.0	0.6	1.4	0.57143	0.14286	0.90906
Sr_2LaNbO_6	Sr	La	Nb	O	1.44	1.032	0.64	1.4	0.59714	0.14	0.89468
Sr_2LaTaO_6	Sr	La	Ta	O	1.44	1.032	0.64	1.4	0.59714	0.14	0.89468
Sr_2LiReO_6	Sr	Li	Re	O	1.44	0.76	0.53	1.4	0.46071	0.08214	0.98045
Sr_2MgMoO_6	Sr	Mg	Mo	O	1.44	0.72	0.59	1.4	0.46786	0.04643	0.97673
Sr_2MgWO_6	Sr	Mg	W	O	1.44	0.72	0.6	1.4	0.47143	0.04286	0.97443
Sr_2NaReO_6	Sr	Na	Re	O	1.44	1.02	0.53	1.4	0.55357	0.175	0.9175
Sr_2ScNbO_6	Sr	Sc	Nb	O	1.44	0.745	0.64	1.4	0.49464	0.0375	0.9594
Sr_2ScTaO_6	Sr	Sc	Ta	O	1.44	0.745	0.64	1.4	0.49464	0.0375	0.9594
Sr_2TiHfO_6	Sr	Ti	Hf	O	1.44	0.605	0.71	1.4	0.46964	0.0375	0.97571
Sr_2TiZrO_6	Sr	Ti	Zr	O	1.44	0.605	0.72	1.4	0.47321	0.04107	0.97329
Sr_2YNbO_6	Sr	Y	Nb	O	1.44	0.9	0.64	1.4	0.55	0.09286	0.92377
Sr_2YTaO_6	Sr	Y	Ta	O	1.44	0.9	0.64	1.4	0.55	0.09286	0.92377
Sr_3MoO_6	Sr	Sr	Mo	O	1.44	1.18	0.59	1.4	0.63214	0.21071	0.87162
Sr_3WO_6	Sr	Sr	W	O	1.44	1.18	0.6	1.4	0.63571	0.20714	0.86999
$Tl_2NaScCl_6$	Tl	Na	Sc	Cl	1.7	1.02	0.745	1.81	0.48757	0.07597	0.9206

Table A.3: Ionic Radii r_A, r_B, r'_B, r_X in Å [31] for the different ions (A,B,B',X) of the different double perovskites and the avergage octahedral factor $\bar{\mu}$, octahedral mismatch $\Delta\mu$ and generalized tolerance factor t (calculated with eq. (5.3), (5.4) and (5.5)).

Bibliography

[1]T. Esswein and N. A. Spaldin, "Ferroelectric, quantum paraelectric, or paraelectric? Calculating the evolution from BaTiO 3 to SrTiO 3 to KTaO 3 using a single-particle quantum mechanical description of the ions", Physical Review Research **4**, 033020 (2022).

[2]M. Filip and F. Giustino, "The Geometric Blueprint of Perovskites", Proceedings of the National Academy of Sciences of the United States of America **115**, 10.1073/pnas.1719179115 (2018).

[3]H. Röhm, "Ferroelektrizität in Methylammoniumbleiiodid-Solarzellen", PhD thesis (Karlsruher Institut für Technologie (KIT), 2019).

[4]K. Momma and F. Izumi, "VESTA 3 for three-dimensional visualization of crystal, volumetric and morphology data", Journal of Applied Crystallography **44**, 1272–1276 (2011).

[5]M. T. Sebastian, "ABO3 TYPE PEROVSKITES", in *Dielectric Materials for Wireless Communication*, edited by M. T. Sebastian (Elsevier, Amsterdam, 2008), pp. 161–203.

[6]A. A. Elbadawi, O. A. Yassin, and M. A. Siddig, "Effect of the Cation Size Disorder at the A-Site on the Structural Properties of SrAFeTiO6 Double Perovskites (A = La, Pr or Nd)", Journal of Materials Science and Chemical Engineering **3**, 21–29 (2015).

[7]X. Cao, L. Kang, S. Guo, M. Zhang, Z. Lin, and J. Gao, "Cs2NaVCl6: A Pb-Free Halide Double Perovskite with Strong Visible and Near-Infrared Light Absorption", ACS Applied Materials & Interfaces **11**, 38648–38653 (2019).

[8]S. S. Nair, L. Krishnia, A. Trukhanov, P. Thakur, and A. Thakur, "Prospect of double perovskite over conventional perovskite in photovoltaic applications", Ceramics International **48**, 34128–34147 (2022).

[9]F. Giustino and F. Giustino, *Materials Modelling using Density Functional Theory: Properties and Predictions* (Oxford University Press, Oxford, New York, 2014).

[10]R. M. Martin, *Electronic Structure: Basic Theory and Practical Methods* (Cambridge University Press, 2020).

[11]P. Hohenberg and W. Kohn, "Inhomogeneous Electron Gas", Physical Review **136**, B864–B871 (1964).

[12]W. Kohn and L. J. Sham, "Self-Consistent Equations Including Exchange and Correlation Effects", Physical Review **140**, A1133–A1138 (1965).

[13]*Planewaves, Pseudopotentials and the LAPW Method* (Springer US, 2006).

[14]D. R. Hamann, M. Schlüter, and C. Chiang, "Norm-Conserving Pseudopotentials", Physical Review Letters **43**, 1494–1497 (1979).

[15]K. F. Garrity, J. W. Bennett, K. M. Rabe, and D. Vanderbilt, "Pseudopotentials for high-throughput DFT calculations", Computational Materials Science **81**, 446–452 (2014).

[16]P. Giannozzi, S. Baroni, N. Bonini, M. Calandra, R. Car, C. Cavazzoni, D. Ceresoli, G. L. Chiarotti, M. Cococcioni, I. Dabo, A. D. Corso, S. de Gironcoli, S. Fabris, G. Fratesi, R. Gebauer, U. Gerstmann, C. Gougoussis, A. Kokalj, M. Lazzeri, L. Martin-Samos, N. Marzari, F. Mauri, R. Mazzarello, S. Paolini, A. Pasquarello, L. Paulatto, C. Sbraccia, S. Scandolo, G. Sclauzero, A. P. Seitsonen, A. Smogunov, P. Umari, and R. M. Wentzcovitch, "QUANTUM ESPRESSO: a modular and open-source software project for quantum simulations of materials", Journal of Physics: Condensed Matter **21**, 395502 (2009).

[17]R. E. Cohen, "Origin of ferroelectricity in perovskite oxides", Nature **358**, 136–138 (1992).

[18]K. Kopitzki and P. Herzog, *Einführung in die Festkörperphysik* (Springer, Berlin, Heidelberg, 2017).

[19]L. Yang, X. Li, E. Allahyarov, Q. Zhang, and L. Zhu, "Novel polymer ferroelectric behavior via crystal isomorphism and the nanoconfinement effect", Polymer **54**, 1709–1728 (2013).

[20]M. Christl, "Charakterisierung ferroelektrischer Eigenschaften von ultradünnen epitaktischen BaTiO3-Schichten mittels Rastersondenuntersuchungen", 10 . 25673 / 2102 (2017).

[21]S. Hunklinger, "Festkörperphysik", in (De Gruyter Oldenbourg, 2017).

[22]N. W. Ashcroft and N. D. Mermin, *Festkörperphysik* (Oldenbourg Wissenschaftsverlag, 2001).

[23]E. Tosatti and R. Martoňák, "Rotational melting in displacive quantum paraelectrics", Solid State Communications **92**, 167–180 (1994).

[24]C. N. R. Rao, "Phase transitions and the chemistry of solids", Accounts of Chemical Research **17**, 83–89 (1984).

[25]T. Esswein, "From Ferroelectricity to Quantum Paraelectricity — Evolution and Doping from First Principles", Doctoral Thesis (ETH Zurich, 2022).

[26]L. D. Landau and E. M. Lifshitz, *Statistical Physics: Volume 5* (Elsevier, 2013).

[27]D. Shin, S. Latini, C. Schäfer, S. A. Sato, U. De Giovannini, H. Hübener, and A. Rubio, "Quantum paraelectric phase of SrTiO3 from first principles", Physical Review B **104**, L060103 (2021).

[28]K. van Benthem, C. Elsässer, and R. French, "Bulk Electronic Structure of SrTiO3: Experiment and Theory", Journal of Applied Physics, v.90, 6156-6164 (2001) **90**, 10.1063/1.1415766 (2001).

[29]L. Bergmann and C. Schaefer, *Lehrbuch der Experimentalphysik / Festkörper* (De Gruyter, Berlin, 2005).

[30]M. E. Wieser and M. Berglund, "Atomic weights of the elements 2007 (IUPAC Technical Report)", Pure and Applied Chemistry **81**, 2131–2156 (2009).

[31]R. D. Shannon, "Revised effective ionic radii and systematic studies of interatomic distances in halides and chalcogenides", Acta Crystallographica Section A: Crystal Physics, Diffraction, Theoretical and General Crystallography **32**, 751–767 (1976).

Erklärung

Hiermit erkläre ich, dass ich die vorliegende Arbeit selbständig angefertigt, an noch keiner anderen Stelle zur Begutachtung eingereicht, keine anderen als die angegebenen Hilfsmittel verwendet und alle wörtlichen oder sinngemäßen Übernahmen von Aussagen bzw. Ergebnissen Dritter an der jeweiligen Stelle meiner Ausführungen kenntlich gemacht sowie alle benutzten Quellen in der Bibliografie aufgelistet habe.

Kiel, den

_____

Unterschrift